Nofima

Automatic quality control of internal defects in cod
Results from hyperspectral, ultrasound and X-ray imaging

Karsten Heia, Kathryn E. Washburn & Martin H. Skjelvareid

Nofima is a business oriented research institute working in research and development for aquaculture, fisheries and food industry in Norway.

Nofima has about 350 employees.

The main office is located in Tromsø, and the research divisions are located in Bergen, Stavanger, Sunndalsøra, Tromsø and Ås.

Company contact information:
Tel: +47 77 62 90 00
E-mail: post@nofima.no
Internet: www.nofima.no

Business reg.no.:
NO 989 278 835 VAT

Main office in Tromsø:
Muninbakken 9–13
P.O.box 6122 Langnes
NO-9291 Tromsø

Ås:
Osloveien 1
P.O.box 210
NO-1433 ÅS

Stavanger:
Måltidets hus, Richard Johnsensgate 4
P.O.box 8034
NO-4068 Stavanger

Bergen:
Kjerreidviken 16
P.O.box 1425 Oasen
NO-5844 Bergen

Sunndalsøra:
Sjølseng
NO-6600 Sunndalsøra

Alta:
Kunnskapsparken, Markedsgata 3
NO-9510 Alta

Report

Summary/recommendation:

Three different technologies were evaluated for the detection of embedded defects in cod fillets: ultrasound, x-ray imaging and the interactance acquisition mode of hyperspectral imaging.

Previous studies had demonstrated interactance hyperspectral imaging to be a promising method to automatically identify nematodes in cod fillets. Improvements had been made to the illumination system that significantly increased the signal to noise ratio since that previous work. The detection rate with the new hyperspectral setup was approximately 40%, less than the former study. This is attributed to the storage time of the fillets as compared to the previous work and also differences in sample handling between the training and test set. Future work needs to be performed on-site in order to avoid results more pessimistic than would be encountered in industrial implementation.

The ultrasound images were noisy and produced too little contrast between the muscle and nematodes, making reliable detection not feasible.

Dual energy ray CT proved capable of detecting deeply embedded nematodes, but it is too slow and expensive for industrial application. Measurements on planar x-ray were inconclusive and require further study. While some high-density spots were observed in the loin in locations where nematodes were located during dissection, not all nematodes were identified and contrast was low.

Summary/recommendation in Norwegian:

Tre ulike teknikker ble testet for påvisning av innvendige defekter i torskefilet: Ultralyd, røntgen avbildning og hyperspektral avbildning i interaktans modus.

Avbildningsoppsettet (interaktans) ble forbedret i forhold til tidligere studier, men deteksjonsraten ble lavere enn tidligere rapportert. Dette skyldes mest sannsynlig at filetene denne gangen ble lagret i ulik tid før måling, mens i tidligere publisert studie ble testing utført i industrien. I fremtidige forsøk må dette tas hensyn til.

Ultralydavbildning ga støyete bilder med lite kontrast mellom kveis og muskel, og ble vurdert som uegnet som metode for deteksjon. Basert på to-energi CT var det mulig å påvise kveis, men teknologien er for tidkrevende og dyr for industriell anvendelse. Forsøk med 2D to-energi røntgen ga ikke entydige svar og vil kreve mere forskning.

Table of Contents

1 Introduction

1.1 About the project

Automation of fish processing has been recognized as a key factor in maintaining strong and competitive fish processing industry within the Nordic countries. Approaches for in-line monitoring of quality of raw material and products are needed to improve production management and optimize throughput and value of products.

Quality grading and inspections are currently done manually and, therefore depend on employee skills, performance may vary each day. Manual evaluation is typically based on selected samples whereas automated quality systems can verify every product. Automated methods can be calibrated and standardized meanwhile there is always a risk of human errors and differences between individual employees with manual inspection. Reducing human error with automated quality control systems also allows companies to focus their human resources on areas of the operation where they can be better utilized.

Among the challenges associated with automated in-line quality grading systems are the high inspection speed needed, detection of defects buried or embedded deep in the fish muscle, varying thickness and size of fillets, whether products are skinned or not, the harsh processing environment and price limits for the measurement equipment needed.

The main purpose of the performed research activities was to develop methods for detection of embedded nematodes, blood spots and bones in whitefish fillets. The quality measurement methods developed in this project will be combined with the methods from the ongoing project on surface defects in a future automatic quality inspection prototype.

As part of the performed research four measurement techniques with potential for measuring internal defects have been tested for nematode, blood and bone detection. Those are hyperspectral imaging, ultrasound, dual-energy X-Ray and NIR transmission. The NIR transmission method was studied by Sintef Digital and is presented in a separate report.

1.2 Nematode detection

Detection of nematodes in fish has been an area of research for decades, and several different approaches have been tested. Readers are referred to (Agnar Holten Sivertsen *et al.*, 2011; Agnar H. Sivertsen *et al.*, 2012; Levsen, Lunestad & Berland, 2005) for overviews of the nematode problem and previous work on nematode detection.

1.3 Hyperspectral imaging

Nofima has worked for several years on developing an industrial solution for hyperspectral imaging of fish products. The technology was included in the project for detection of nematodes and blood. In hyperspectral imaging, each pixel of the image contains high-resolution information on light intensity as a function of wavelength (a "spectrum"). This can be compared to a color camera, which only registers light intensity in three broad wavelength ranges ("red","green" and "blue"). The high-

resolution spectral information in hyperspectral images can for example be used to identify specific objects or chemicals by analysis of structure or spectral characteristics.

In the work presented here, a push-broom camera was used operated in interactance mode. Imaging in interactance mode forces the light to travel some distance into the fish muscle before being re-emitted at the surface and measured. This camera images the fillets "one line at a time" as they move past on a conveyor belt. The illumination and imaging concept is visualized, as shown in Figure 1.
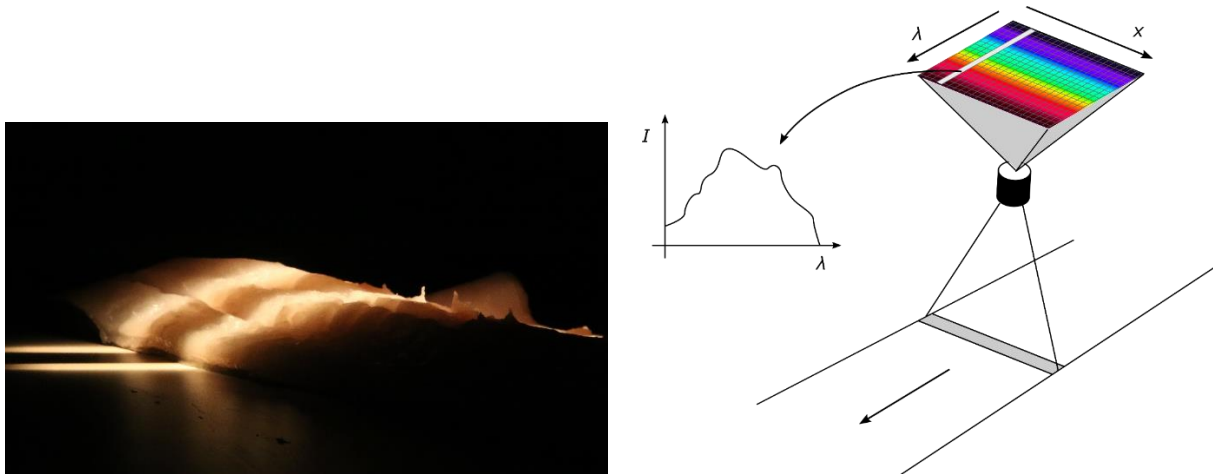
Figure 1   Left side: Image of cod fillet illuminated with two light lines where the measurement is performed in the middle between the lines. Right image: Concept of hyperspectral camera, image one spatial line at time with full spectral information.

As part of another project with Norway Seafoods and Marel, two cabinets have been designed and tested for making the imaging setup more industry deployable. For the illumination for interactance imaging, the fiber line and focusing element has been redesigned to get a more focused light line. This allows the light lines to be positioned closer to the measurement line without projecting light directly into the measurement area, increasing the measured signal to noise.

The most recent publication from Nofima regarding hyperspectral imaging for nematode detection is (Agnar H. Sivertsen *et al.*, 2012). The work described in this report differs from that in the paper in the following ways:

- PCA analysis is included for data reduction and extraction of relevant features
- Several variations of pre-processing (both spatial and spectral) are tested, both individually and merged
- A simplified system with fewer spectral channels is simulated and evaluated

1.4   Ultrasound

Ultrasound was included as a potential method for detecting nematodes deeply embedded in fish muscle tissue. Ultrasound has a much lower degree of scattering in fish muscle than e.g. visible light, and can therefore penetrate several centimeters into biological tissue.

Nofima has previously conducted some preliminary experiments with ultrasound imaging of nematodes which were "implanted" in cod fillets, using an ultrasound transmission setup. The

conclusions from these tests were that in some cases, there was a visible but weak contrast between fish muscle and nematodes. Muscle structures represented a type of "background noise" in the images. The transmission imaging method was also very time-consuming, and would be difficult to integrate as part of a conveyor belt setup in an industrial system.

For the study described in this report, a commercial ultrasound imaging instrument with real-time imaging was used. The instrument operates in a pulse-echo imaging mode, which only requires access to one side of the fillet. This imaging mode is seen as a better candidate for implementation in an industrial system.

1.5 Dual-energy X-ray

Dual-energy X-ray CT was investigated as a possible method to detect nematodes far below the surface of the fillet. X-ray imaging has the advantage that it has a large depth of penetration compared to other measurement techniques. However, earlier studies using X-rays by other researchers found the contrast between nematode and muscle was too low to enable detection. To try to overcome this problem, in this study a relatively new technique, dual-energy X-ray imaging, was used to enhance contrast in X-ray images in an attempt to identify nematodes.

Nofima conducted preliminary experiments in conjunction with the Universitetssykehuset Nord-Norge using a commercial medical dual-energy X-ray CT system. The experiments yielded promising results to distinguish nematodes from the surrounding tissue but both measurement time and equipment cost were too great to be feasible for wide scale application.

Further testing was performed using a planar X-ray system at the Universitetssykehuset Nord-Norge. Results were inconclusive. Due to saturation of the detector, nematodes in the belly of the fish could not be identified. Several high-density spots were observed in images of the loin in areas near where nematodes were found during dissection. Additional testing with different equipment or acquisition parameters may give improved results.

2 Hyperspectral imaging – methods and results

2.1 Instrumentation – interactance mode hyperspectral imaging

2.1.1 Illumination and hyperspectral camera

Imaging was performed with a pushbroom hyperspectral camera with a spectral range of 410-1000 nm and spatial resolution of 0.3 mm across-track by 0.6 mm along track (Norsk Elektro Optikk, model VNIR-1024). The camera was fitted with a lens focused at 1000 mm, mounted 1020 mm above a conveyor belt. Samples were illuminated using two custom made fiber optic line lights (Fiberoptics Technology Inc. Connecticut, USA), fitted with custom made collimating lenses yielding light lines approximately 5 mm wide (Optec S.P.A., Milano, Italy). Each line light was 400 mm wide, with six bundles of optical fibers. The light from 12 focused 150 W halogen lamps with aluminium reflectors (International Light Technologies, Massachusetts, USA, model L1090) was fed into the fiberoptic bundles, representing a total 1800 W of electrical input power. The imaging and illumination setup is shown in Figure 2.
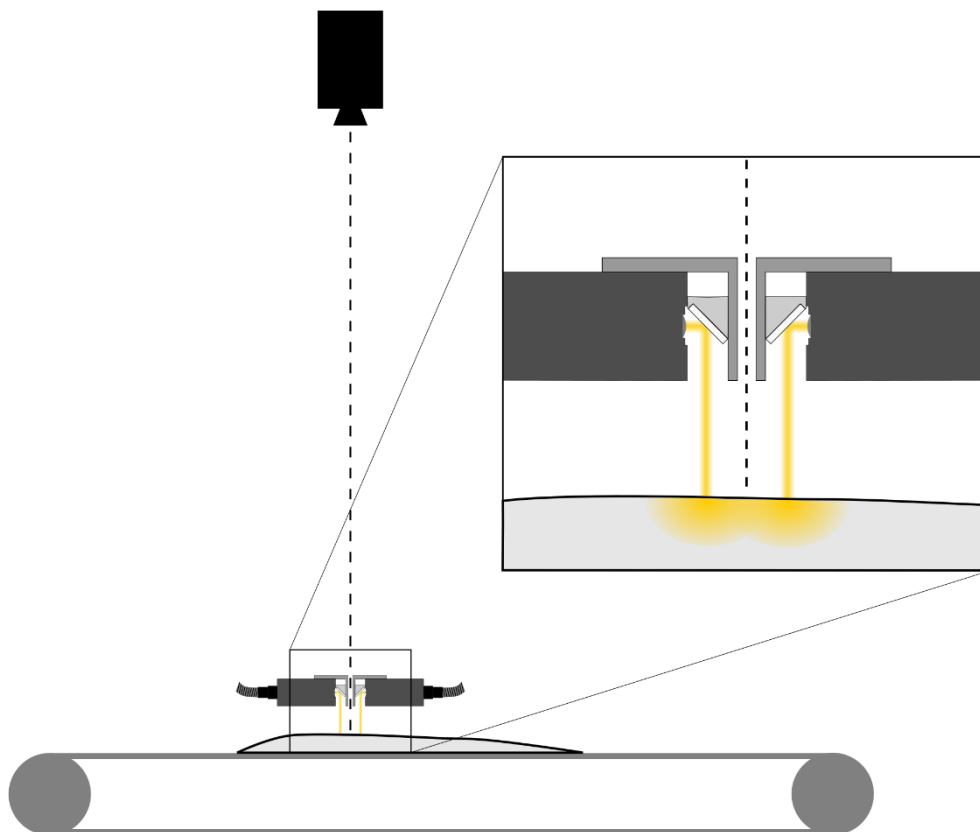

Figure 2   Hyperspectral camera, conveyor belt and fiberoptic line lights used for interactance mode imaging. The light is reflected via mirrors and down on to the sample. The hyperspectral camera's line of view is placed directly between the two light lines. The transport of light from the light lines to the measurement area is due to scattering inside the sample.

2.1.2　Image calibration – interactance

A 25 mm thick plate of polytetrafluoroethylene (PTFE, also known as Teflon) was used to create a reference image prior to each imaging session. The physical characteristics of PTFE remain stable over time, and thus images of the PTFE can be used to measure and correct for changes in illumination and camera sensitivity over time.

A reference corrected image $I_{CORR}(x, y, \lambda)$ was calculated from a raw hyperspectral image $I_{RAW}(x, y, \lambda)$ using the following formula:

$$I_{CORR}(x, y, \lambda) = \frac{I_{RAW}(x, y, \lambda) - B(x, \lambda)}{\bar{I}_{TEF}(x, \lambda) - B(x, \lambda)}$$

where $B(x, \lambda)$ is the "dark current" background level (camera response with no light input) and $\bar{I}_{TEF}(x, \lambda)$ is the raw image of the Teflon plate, averaged along the conveyor belt direction y.

2.2　Methods for nematode detection

2.2.1　Manual marking of nematodes in images

During experiments, fillets were first imaged and then manually inspected for nematodes. The nematodes were then marked in the hyperspectral images as ROIs (regions of interest). The following types of ROIs were marked in each image

- Visible nematodes (accurately marked, pixel-by-pixel)
- Non-visible nematodes (marked as a larger area, since exact position was unknown)
- Belly (always 2 ROIs)
- Loin (always 2 ROIs)
- Tail (always 2 ROIs)
- Center line with blood (always 2 ROIs)

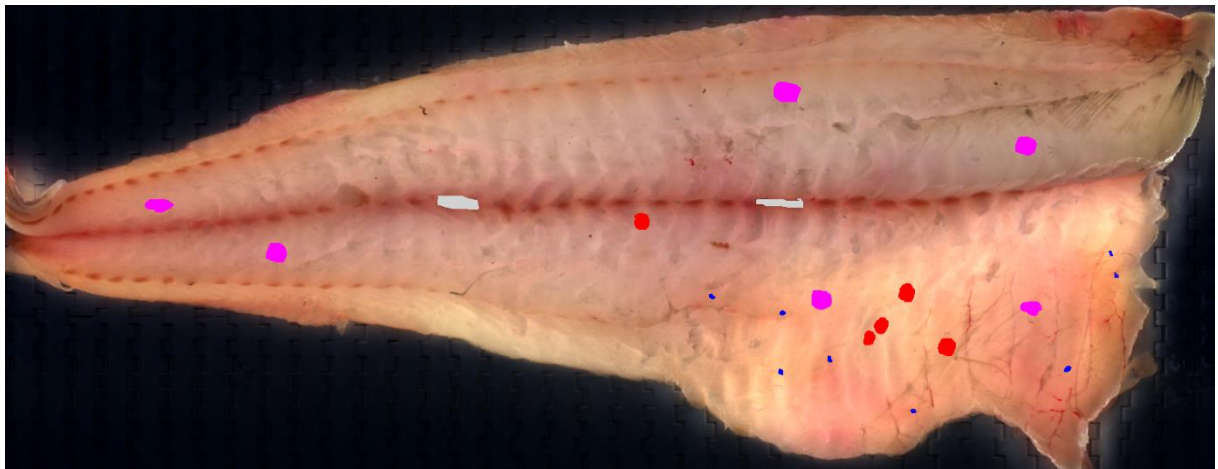An example image with ROIs indicated is shown in Figure 3.

Figure 3　Example of ROIs marked on interactance image. Blue – visible nematodes, red – non-visible nematodes, magenta – muscle (belly, loin, tail), light gray – center line (blood).

2.2.2 Spectral pre-processing

Pre-processing of spectra is often employed in analysis of hyperspectral images (and spectroscopy in general) to remove unwanted variation in the data while retaining as much of the useful information as possible. For example, local variations in illumination or scattering can cause variations in light intensity that are unrelated to the target of the analysis (nematodes, in this case). Three well-known pre-processing methods were tested, in addition to using the raw spectra (no pre-processing):

- Normalizing the area under the spectral curve
- Scaling and shifting the spectrum to have a standard deviation of 1 and zero mean ("standard normal variate transform")
- Numerical derivation of the spectrum (calculating differences between neighboring samples)

The full spectral range of the VNIR-1024 hyperspectral camera is 410-1000 nm. From this range, two different wavelength regions were selected for analysis:

- 450-950 nm
- 450-650 nm

The 450-950 nm range corresponds to the "full" spectrum, excluding the end sections of the spectrum with poor signal-to-noise ratio. The 450-650 nm range corresponds to the part of the spectrum displaying the highest contrast between nematode and muscle (Stormo et al. 2007).

2.2.3 Down-sampling of dataset to simulate simpler measurement setup

In addition to using the full hyperspectral datasets as described above, simplified datasets were also included for comparison. These datasets were created by resampling the hyperspectral data, simulating a hyperspectral system where each channel had a spectral FWHM ("full width half maximum") spectral response of 10 nm, with channels centered on wavelengths 450, 470, 490, 510, 530, 550, 570, 590, 610, 630, 650, 700, 750, 850. The spectrum was sampled more closely at the shortest wavelengths (450-650 nm) than at the longer wavelengths (700, 750, 850 nm), since it was observed from raw data that the contrast between nematodes and muscle was highest at the shortest wavelengths. The PCA model coefficients (see Section 9.1) also show that there are more spectral "structures" in the 450-640 nm range. A spectral resolution of 20 nm was considered enough to capture the main variations in these structures. At wavelengths above 650 nm, there is less spectral structure, and in this range the samples were therefore limited to 700, 750 and 850 nm.

The full spectral range was kept within a single octave, since this generally leads to a simpler hyperspectral system. The 450-750 nm range corresponds approximately to the range covered by a white LED system, and the 850 nm wavelength was included specifically because this is a common wavelength for infrared LEDs.

In total, the resampled datasets represent data which could be acquired using LED illumination and a simplified hyperspectral camera with only 14 channels. Relative to the full hyperspectral image, this represents a reduction in data size by a factor of approximately 15.

2.2.4   PCA analysis

Principal component analysis (PCA) was employed in the analysis of the images, with a twofold purpose:

1. To extract features from the images which are relevant for nematode detection
2. To reduce the dimensionality of the data and speed up nematode detection algorithms

PCA models were based on data from the ROIs in the images. All spectra from visible nematodes were included in the model training set. For each fish, these spectra were set to constitute 20 % of all the spectra used. An equal number of spectra was chosen randomly from the belly, loin, tail and center line classes. Thus, the training data set was balanced, with 20 % of the spectra from each class.

The PCA models were then applied to all of the data in each hyperspectral image, yielding images with 7 image planes corresponding to the 7 first principal components.

2.2.5   High-pass filtering

With interactance imaging, the light that interacts with a nematode also interacts with the muscle that the nematode is embedded in. Thus, the light measured at the position of a nematode is a mix between the nematode spectrum and the muscle "background". To remove the effects of the local background, and to enhance the contrast between the nematodes and the muscle, the PCA images were high-pass filtered. An example of a high-pass filtered image is shown in Figure 4b). High-pass filtering was performed by smoothing each image plane with a Gaussian kernel with sigma corresponding to 3 mm (the smoothing effect is similar to averaging using a disk with 6 mm diameter).
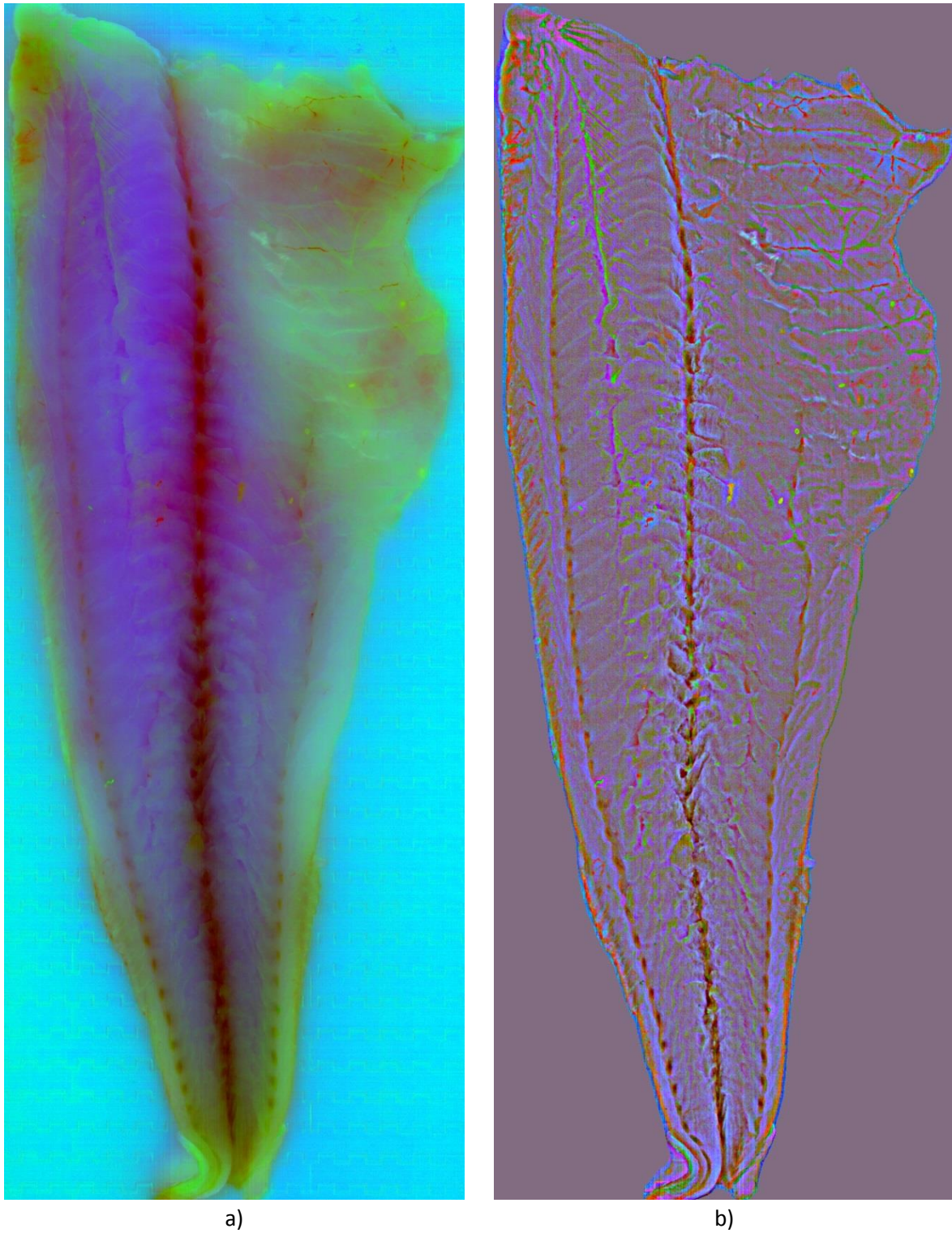
Figure 4   Example of PCA image (fillet B04 imaged on 2016-11-04, area normalized spectra, 450-950 nm). Principal components 1-3 are mapped to the blue, green and red color channels, respectively. The original PCA image is shown in a), and in b), a high-pass filtered version is shown. The green specks in the belly area correspond to nematodes. –But not those in loin, tail?

2.2.6   Image classification for nematode detection

Image classification is performed by taking a training set where the categorization of different spectra is known. This training set is used to create a model to relate the spectra to their classifications. The model is then applied to predict the categorization of unknown spectra in hyperspectral images. Several classification methods of the pre-processed spectra were evaluated: k-nearest neighbours, linear discriminant analysis, quadratic discriminant analysis, and support vector machines.

The K-nearest neighbours (KNN) method functions by taking a calibration set of samples with both a variable space and a classification. Then each new sample is classified based on the closest neighbour or neighbours in the variable space. For example, for k=1, classification of a new sample would be determined by the nearest sample in the variable space while for k=3, classification of the new sample would be determined by the classification of the three nearest samples in the variable space. A drawback of the method is computation time. For very large classification sets, calculation time can be extensive. This can be mitigated by limiting the size of the classification set. The method can also be prone to instability, particularly if k is small.

Linear discriminant analysis (LDA) takes in samples with a variable space and a classification. The method is similar to a PCA in that it is a linear transformation method to describe the variance in the data set. Whereas the PCA describes the variance in the sample data, the LDA describes the variance between the different classes to create hyperplanes to separate the different categories. The method is quick compared to KNN and SVM (support vector machines) analysis. The method is also generally stable and less prone to overfitting.

Quadratic discriminant analysis (QDA) was also investigated as a possible classification method. It is similar to linear discriminant analysis except instead of hyperplanes, the categories are separated by quadratic surfaces. This generally allows a better separation of the categories in the training set. However, this approach appeared to be very prone to overfitting when applied to new data. Therefore, this approach was quickly discarded in early testing.

The final classification method investigated was support vector machines (SVM). SVM has the advantage of being a non-discrete classification technique. Whereas the other methods force a sample to belong to a distinct category, the SVM allows a fuzzy classification. This enables an evaluation of how well a particular sample resembles a particular category and to control how close it needs to be to the category center before it is accepted as a true member of the category.

In addition to classification methods, two different calibration set inputs were investigated. First, all spectra from the selected ROI were used to create the calibration set. In order to prevent computation time from becoming excessive, two thousand spectra were randomly extracted and used as calibration set for the KNN and SVM classifications. The second approach involved filtering, or "cleaning", the spectra in the training set. The selection of the ROI was performed manually and therefore the selected spectra may be more or less representative of the category they are intended to define. The data in the calibration sets were cross validated using the classification approach to be applied to new images and any spectra that were not classified in the correct categories were removed from the calibration set.

2.2.7   Spatial Filtering of Objects Classified as Nematodes

In order to decrease the number of false positives, several methods of spatially filtering the classified images were undertaken. Because nematodes have a certain size range, boundaries were set on the object sizes that could reasonably be nematodes. Objects that were too small were assumed to be noise and were removed. Similarly, very large objects that were too large to be nematodes likely arose from misclassification of a filet feature (e.g. blood clot), and therefore were also removed. It was found that the presence of the black lining produced many false positives in the images. As this is a quality defect that requires trimming, portions of the image containing black lining were removed from classification. While filtering by object shape was investigated, it was found that false positives were of very similar shape to real nematodes and shape filtering would not improve results. Lastly, because the training set was developed on *Anasakis simplex*, only predictions in regions of the fish where anasakis reside needed to be considered. Thus, the classified images were filtered such that any nematode predictions outside the belly of the fish were removed. For an eventual *Pseudoterranova decipiens* model, because the species of nematode can reside anywhere in the fillet, this type of filtering could not be applied.

An additional approach to minimize false positives involved combining two or more classified images. Here, two classifications are compared and only areas that are classified as nematode in both images are kept. The mechanism behind this is that different classification methods have a tendency to produce different types of false positives. Therefore, combining images from two or more different classification types can lower the true false positive rate. However, a drawback to the approach is that it tends to lower the overall detection rate.

2.2.8   Classification Accuracy and Quality

After classification and spatial filtering, the quality of the different classification methods was evaluated to determine how well each one performed.

The initial evaluation method attempted was purely pixel based; each pixel that had been classified as a nematode was compared to the pixels marked as nematode by manual ROI definition. Pixels that overlapped in the two sets were classified as correct. Pixels that were classified as nematodes, but not in a location defined as part of a nematode ROI were classified as false positive. Pixels that had been identified as nematodes by manual ROI definition that had not been predicted by the algorithm were classified as false negatives. However, frequently there was not complete agreement between which pixels had manually been marked as nematodes and pixels classified by the algorithms as nematode. Therefore, even though for all practical purposes the nematode had been identified by the algorithm, there would be associated false negatives and false positives, as shown in Figure 5.

Pixel Based vs Object Based Classification

Pixel Based   Object Based

■ Correct
■ False Positive
■ False Negative
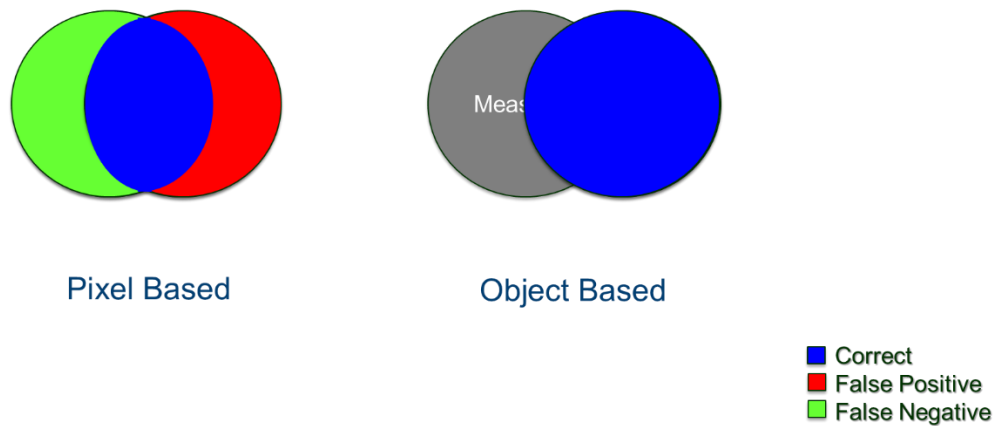
Figure 5   Example of Pixel based classification versus object based. In pixel based classification, any mismatch between the manual marking of a nematode and the predicted pixels were marked as false negative and false positive. For object based classification, any overlap between the two objects resulted in a correct classification

To rectify this problem, the analysis method was revised to be object based. Here adjacent pixels are combined into objects. Then, for any overlap between a predicted object and a measured object, the whole object is assigned as a correct identification. If there is no overlap in the predicted object with a manually marked object, it is assigned as a false positive. Similarly, if there is no overlap of a manually assigned object with a predicted object, it is assigned as a false negative.

At the end of classification, an image was created showing correct identifications, false negatives and false positives, as shown in Figure 6. For each combination of pre-processing and classification method, a statistics file summarizing the number of true positives, false positives and false negatives was created.

■ Correct
■ False Positive
■ False Negative

Figure 6   Example of a classified image (fillet E04 imaged on 2016-11-04, no-preprocessing, 450-950 nm).

2.2.9 Detection statistics

After classification, the quality of the classification was evaluated in several methods. The quality metrics presented in the detection statistics tables are as follows: The overall nematode detection rate was calculated. The detection rate of visible is the percent of the nematodes found by the trimmer that have been identified by the algorithm. The detection rate of nonvisible is the percent of the nematodes not found by the trimmer that hav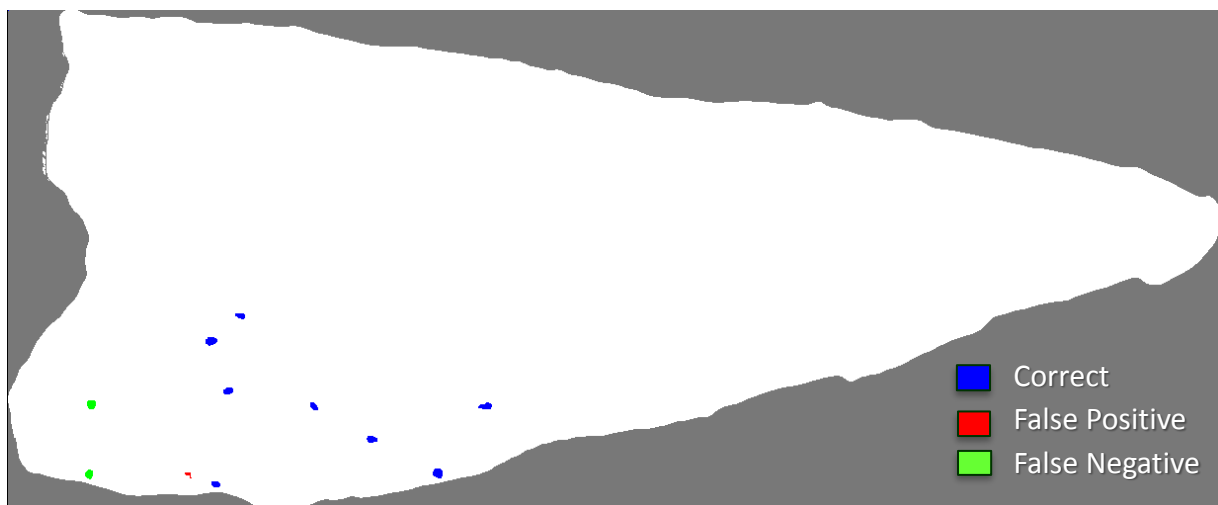e been identified by the algorithm. Average number of false positives describes the average number of false positives per fillet. Lastly, the number of fillets without false positives was calculated.

2.3 Blood detection

After performing the image calibration outlined in section 2.1.2, the spectral readings were transformed into absorbance, $A(x, y, \lambda) = -\ln(I_{CORR}(x, y, \lambda))$.

Based on the constrained spectral un-mixing approach described in Skjelvareid et al. (2017), the blood level and distribution for each fillet was estimated. The following steps are needed to obtain the blood estimate:

1. Find by constrained spectral un-mixing the abundancies for blood (oxy-, deoxy- and met-hemoglobin), water, purified fish muscle.

2. Using a model for transforming the blood abundancies into blood level [mg/g muscle].

2.4 Experiments – methods and materials

2.4.1 Experiment on November 4th 2016 (training data)

50 fillets with nematodes were selected at the Lerøy Norway Seafoods landing facility in Båtsfjord on November 2nd, packed in styrofoam boxes with ice, shipped to Nofima with the costal express, and imaged in the hyperspectral setup on November 4th and 7th. The fish were then vacuum packed and put into frozen storage at -30°C. The fish was frozen for two reasons: First, it enabled a more flexible planning of the manual inspection of the fish, and second, the freezing enhances the fluorescent properties of the nematodes, yielding a high contrast relative to the fish flesh when illuminated with UV light (Pippy 1970).

On November 22nd, the fish was thawed in running water, unpacked, imaged using a diffuse LED UV light (Metaphase Exolight-ISO2-19-UV365-24) and a DSLR camera (Canon EOS 70D). The images were uploaded to a computer, adjusted for increased contrast, printed on paper, and used for marking nematodes during manual inspection of the fish. These notes were later used for marking nematodes in hyperspectral images. An example fluorescence image is shown in Figure 7. Note that this is a "best case" example with most of the nematodes clearly visible.

The fillets contained mainly nematodes of the species *Anisakis Simplex* (small and pale), and only one fillet contained nematodes of the species *Pseudoterranova decipiens* (larger and dark).
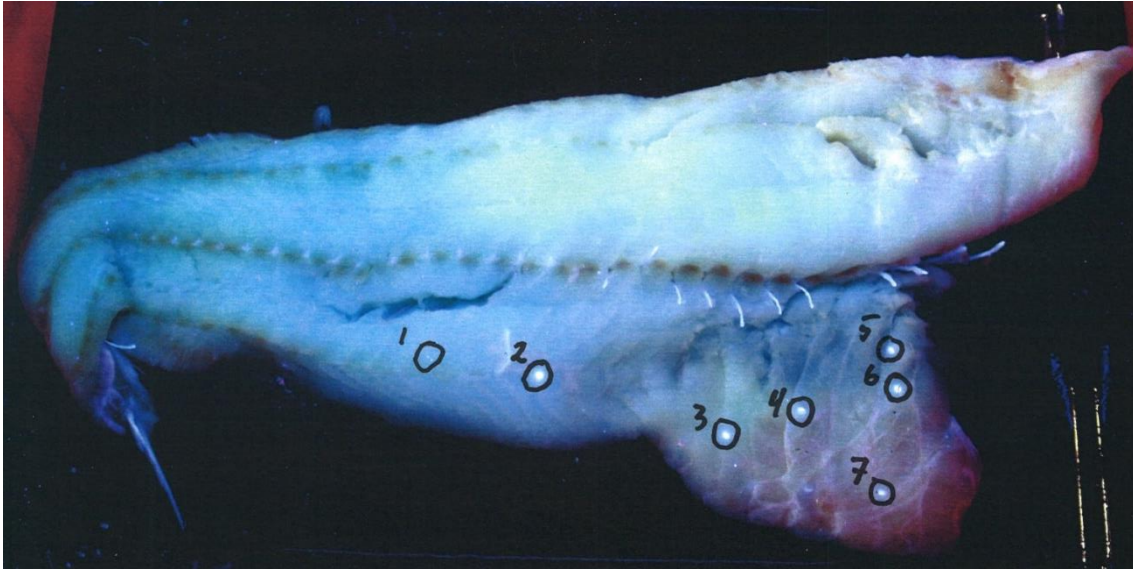
Figure 7   Example of fluorescence image with handwritten notes indicating nematodes. All nematodes except number 1 are visible as bright spots. Note, in addition to the nematodes, bones also strongly fluoresce when illuminated with UV light Maybe also a comment on fluorescent bones – just to clarify?

2.4.2   Joint test with Sintef on May 11th-12th 2017

Nofima originally asked for a shipment of fillets with nematodes for a "pre-test", in order to adapt the analysis of hyperspectral images to detection of *Pseudoterranova Decipiens* ("sealworm") before the joint test with Sintef. *Pseudoterranova Decipiens* is darker and larger than the *Anisakis Simplex* which was observed in the experiment on November 4th 2016. However, Lerøy Norway Seafoods was not able to supply any fillets with nematodes until the same week as the joint test (too early in season).

The "pre-test" samples consisted of 18 fillets from fish landed at the Lerøy Norway Seafoods facility at Forsøl on Friday May 5th 2017. These fillets were packed on ice, shipped to Nofima and imaged on Tuesday May 9th.

The fillets for the joint test consisted of 13 fillets from fish landed at the Lerøy Norway Seafoods facility in Kjøllefjord on Monday May 8th. However, since the number of samples was so low, it was decided to merge these with the "pre-test" samples. The pre-test samples were assigned labels under groups A and B (9 in each groups), and the remaining samples were assigned labels under groups C and D (9 fillet in C, 4 in D).

Imaging for the joint test was performed on Thursday May 11th. At this point, the fillets in group A and B were 6 days old, and the fillets in group C and D were 3 days old.

During the joint test, imaging and inspection of the fillets was performed as shown in Figure 8. Each group was first imaged using interactance and fluorescence imaging. Then simple color images based on data from 440, 518 and 555 nm in the fluorescence images were exported and printed. Fluorescence images were used because the nematodes display a higher contrast relative to the fish muscle, compared to the interactance images (in raw data). The printed images were used for evaluating which fillets should be imaged by Sintef (only fillets with several nematodes), and for marking nematode position during screening by trimmer / thorough manual inspection.
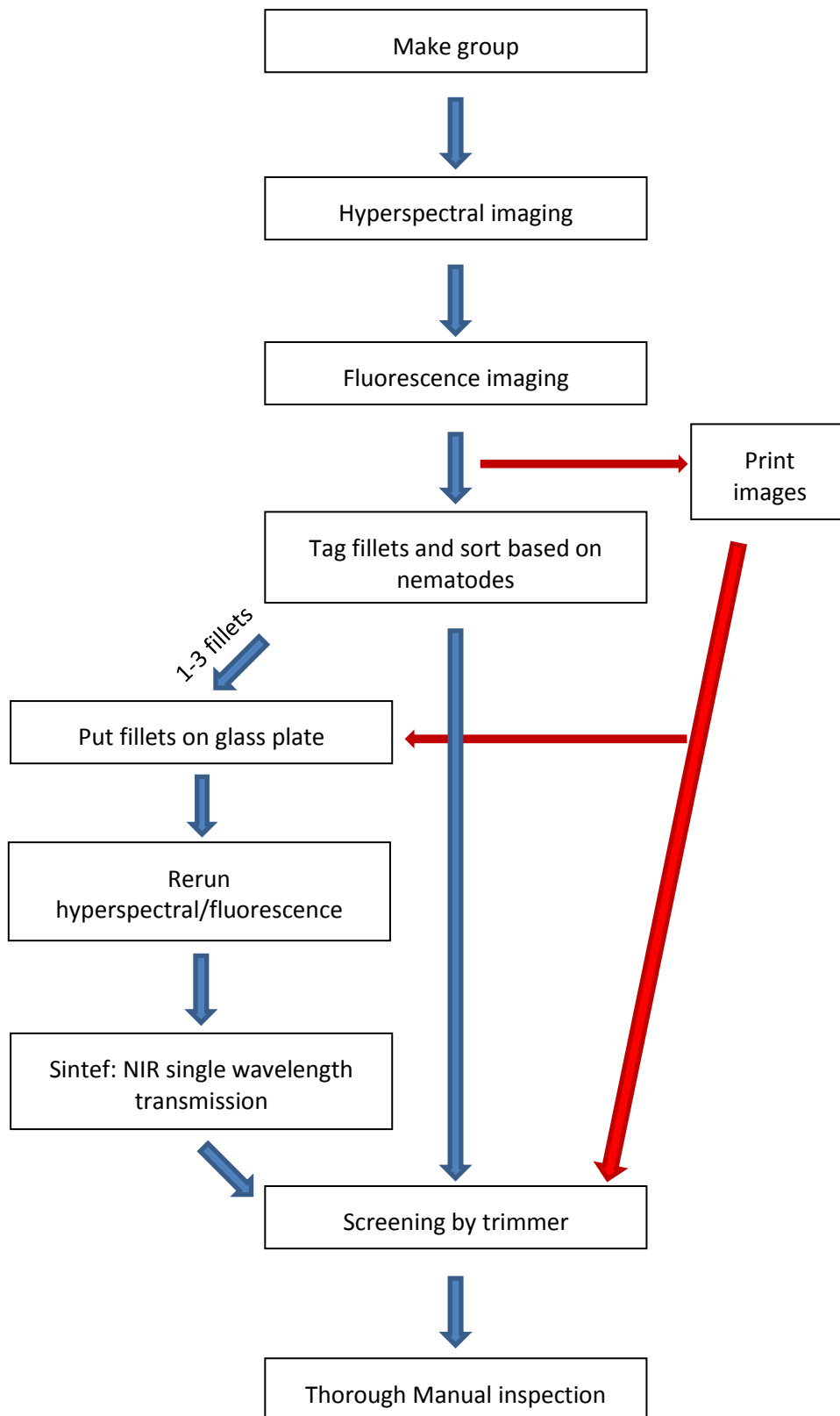
```
                        ┌─────────────────────┐
                        │     Make group      │
                        └─────────────────────┘
                                  │
                                  ▼
                        ┌─────────────────────┐
                        │ Hyperspectral imaging│
                        └─────────────────────┘
                                  │
                                  ▼
                        ┌─────────────────────┐
                        │ Fluorescence imaging │────────────►┌──────────┐
                        └─────────────────────┘             │  Print   │
                                  │                          │  images  │
                                  ▼                          └──────────┘
                        ┌─────────────────────┐                   │
                        │ Tag fillets and sort │                   │
                        │  based on nematodes  │                   │
                        └─────────────────────┘                   │
                     1-3 fillets │                                 │
                          ▼       │                                │
          ┌─────────────────────┐ │◄──────────────────────────────┘
          │ Put fillets on glass │
          │       plate          │
          └─────────────────────┘
                   │
                   ▼
          ┌─────────────────────┐
          │       Rerun          │
          │hyperspectral/fluorescence│
          └─────────────────────┘
                   │
                   ▼
          ┌─────────────────────┐
          │Sintef: NIR single    │
          │wavelength transmission│
          └─────────────────────┘
                   │
                   ▼        │                    │
                 ┌─────────────────────┐
                 │ Screening by trimmer │
                 └─────────────────────┘
                          │
                          ▼
                 ┌─────────────────────┐
                 │Thorough Manual inspection│
                 └─────────────────────┘
```

Figure 8   Workflow during joint test with Sintef

2.5 Results – nematode detection

2.5.1 Trimmer Detections Statistics

Dissection of the 31 fillets after all measurements were complete found a total of 199 nematodes, the majority of which were the species *Anisakis Simplex.* Of these 199 nematodes, 131 nematodes were identified by the trimmer. This gives a 65.8% trimmer detection rate for this study.
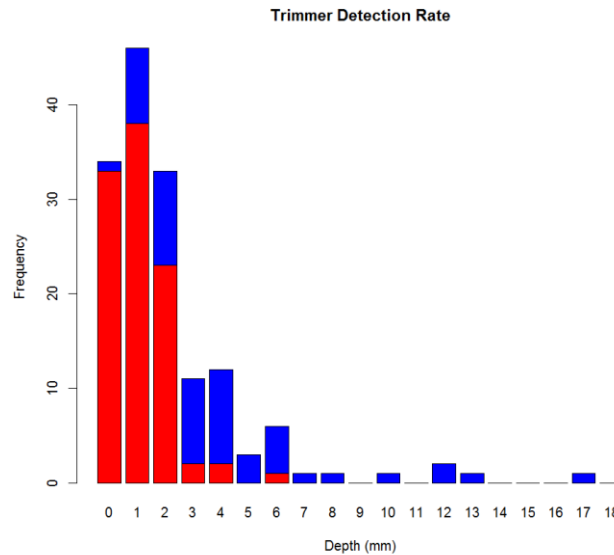

Figure 9   Nematode distribution and trimmer detection rate as a function of depth. Red color indicates nematodes detected, blue color indicates nematodes not detected. The total height of each bar corresponds to the total number of nematodes at each depth.

2.5.2 Hyperspectral Detection Statistics

While some methods performed marginally better than others, overall classification performance was typically similar regardless of preprocessing and classification approaches. An exception is for the data that was first high-pass filtered and then subsequently analysed by PCA. While the method performed well on the training data, the detection results were significantly worse on the test data. A complete description of the classification statistics can be found in the Appendix. For the top performing methods, further evaluation of analysis method was performed. The statistics for the top two methods are given in Table 1. Best methods were selected through evaluation of the ratio between detection rate and the square root of false positives, as well as considering the number of false positive free fillets.

The best two performing methods were both on the data that had been area normalized, decomposed into principal components, and then high pass filtered. The first, LDA classification of the data with a minimum nematode threshold size of 10 pixels produced the best compromise between detection rate and the number of false positives present. Decreasing the minimum nematode size threshold improved detection rates at the expense of a higher number of false positives. A combined LDA-SVM classification with a minimum nematode threshold size of 10 pixels produced the highest number of false positive free fillets at a minor expense to the detection rate. Decreasing the minimum nematode

threshold size did not appear to improve the detection rate but did increase the number of false positives.

Table 1   Statistics for two best performing detection methods

Method	Detection rate (%)	Detection rate - nematodes visible by trimmer **(%)**	Detection rate - nematodes not **visible by trimmer (%)**	Average number of false **positives per fillet**	Number of fillets without false positive (of 31 total)
LDA	41.4	55.9	11.3	6.5	2
LDA+SVM	37.7	51.4	9.4	3.2	4

2.5.3   Detection rate as a function of depth

Figure 10 shows detection rate as a function of nematode depth inside the fish fillet (depth relative to surface imaged), for the two best performing classification methods. The results are nearly identical, but slightly better for the LDA detector. Most nematodes were located at 4 mm or less, and there is a trend for higher detection rate at shallow depths, as would be expected. As with the trimmer detection, none of the nematodes at 7 mm or more were detected. Note however that there were very few deeply embedded nematodes, and the statistics for this depth range may therefore be unreliable.

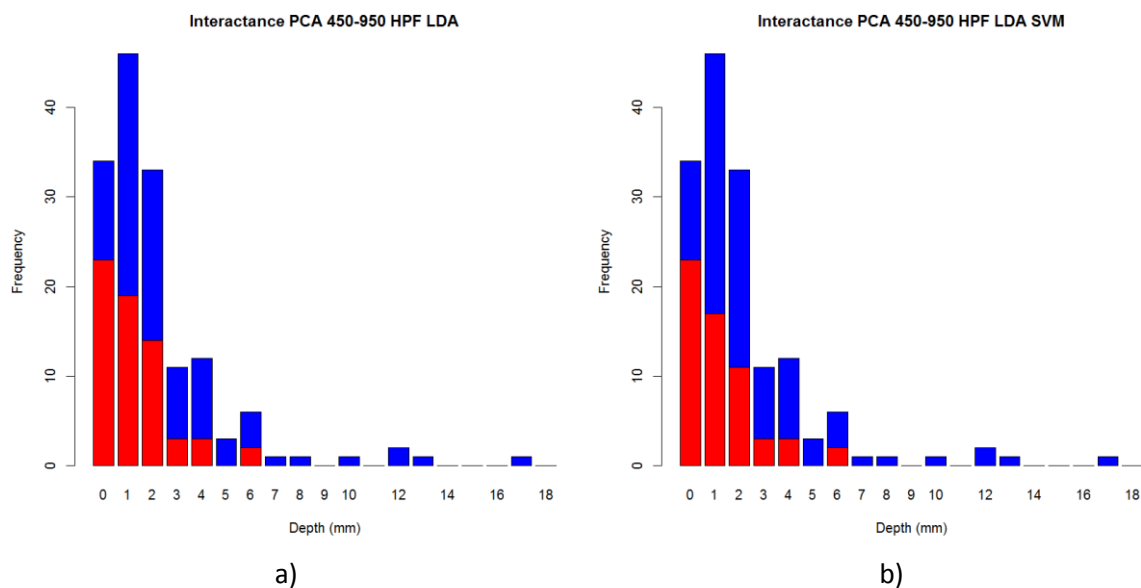a)   b)

Figure 10   Nematode distribution and detection rate as a function of depth. a) Results for LDA classifier. b) Results for combined results from LDA and SVM classifier. Red color indicates nematodes detected, blue color indicates nematodes not detected. The total height of each bar corresponds to the total number of nematodes at each depth.

2.5.4   Detection rate as a function of size

Figure 11 shows detection rate as a function of nematode size, for the two best performing classification methods. The majority of nematodes were 4 mm or less in diameter, reflecting the fact that the majority of nematodes belonged to the *Anisakis simplex* species. There is a slight trend for larger nematodes to be detected more frequently than smaller ones.
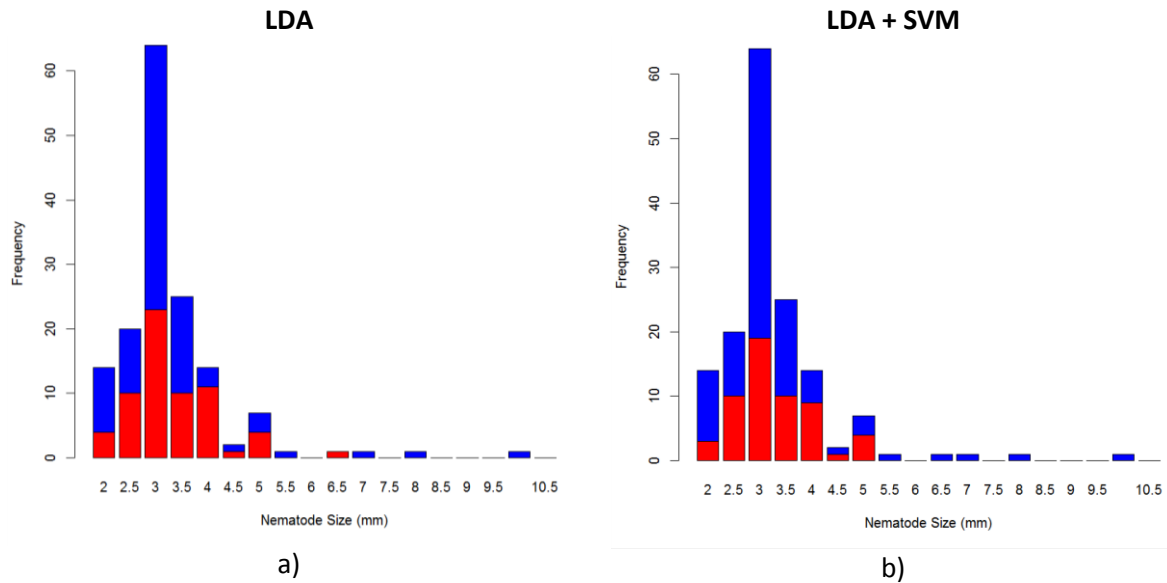
LDA   **LDA + SVM**

a)   b)

Figure 11   Nematode distribution and detection rate as a function of size. a) Results for LDA classifier. b) Results for combined results from LDA and SVM classifier. Red color indicates nematodes detected, blue color indicates nematodes not detected. The total height of each bar corresponds to the total number of nematodes for each size.

2.5.5   Nematode Detection as a function of size and depth

Figure 12 shows the relationship between nematode depth, size and detection rate. The more opaque a point is, the more nematodes have that combination of size and depth. Predominantly red points indicate the all or most nematodes were detected. Predominantly blue points indicate the all or most nematodes were not detected. Purple indicates a mix of detection rate.
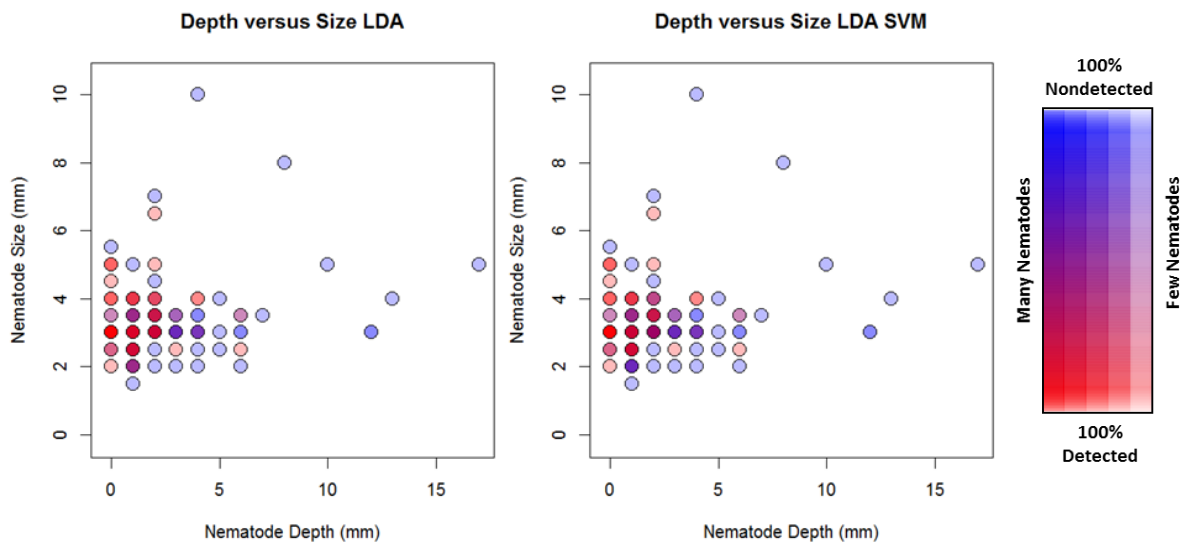

Figure 12   Nematode detection rate as a function of nematode depth and size a) Results for LDA classifier and b) Results for combined results from LDA and SVM classifier. Red color indicates nematodes detected, blue color indicates nematodes not detected.

The detected nematodes predominantly were shallow and small, though these also constituted the majority of nematodes present. Both larger and more deeply buried nematodes were less abundant.

17

This is a reflection that the majority of nematodes present in the samples were *Anisakis simplex,* which tend to be smaller and buried less deeply in the flesh. Despite the larger size of some of the more deeply buried nematodes, they did not appear to be detectable.
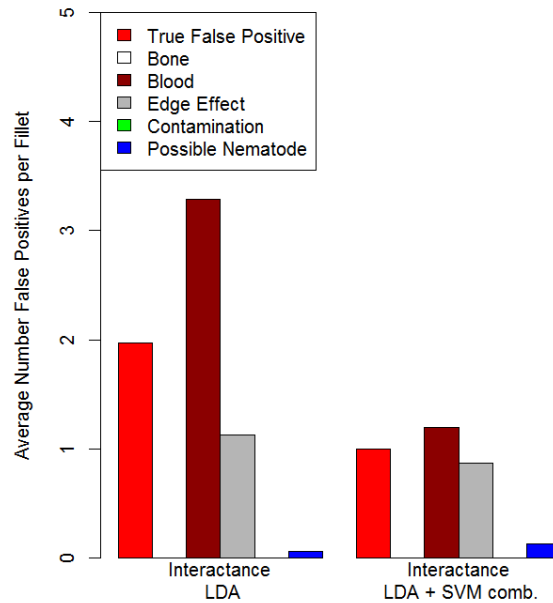
2.5.6   Sources of False Positives

Figure 13   Sources of false positive nematode classifications for the two classification methods

Figure 13 shows the different types of false positives that arise in the classified images. The largest sources of false positives in the images appeared to arise from the misclassification of blood as nematode. By combining the nematode analysis with the blood detection algorithm, it is expected the number of these types of false positives can be reduced. Edge effects also appeared to be a source of some false positives. For pixels that are on the edge of the fillet, their spectra pixels may be a mix of the fillet and conveyor belt, which then appears to be identified by the classifiers as nematode. Furthermore, there were some instances where data strongly indicated there had been a nematode during imaging, but it may have been lost afterwards due to sample handling before the final dissection of the fillets. It is anticipated that with further work, these sources of false positives can be minimized or possibly eliminated. With these sources removed, the remaining average number of false positives were on average about 2 per fillet for the LDA classification and 1 per fillet for the combined LDA and SVM classification.

2.6   Resampled data analysis

To investigate the effect of using a limited number of wavelengths – as may be useful to help minimise costs in an industrial setting - the full spectral data was resampled. The chosen wavelengths were: 450, 470, 490, 510, 530, 550, 570, 590, 610, 630, 650, 700, 750, and 850 nanometers. After resampling, the data was preprocessed, PCA analyzed and high-pass filtered.

Table 2   Statistics for the full and resampled interactance datasets.

Method	Detection rate (%)	Detection rate - nematodes visible by trimmer **(%)**	Detection rate - nematodes not visible by trimmer **(%)**	Average number of false positives per fillet	Number of fillets without false positive (of 31 total)
LDA Full	41.4	55.9	11.3	6.5	2
LDA Resampled	41.3	56.8	9.4	4.3	3
SVM Full	46.3	59.6	18.8	25.6	0
SVM Resampled	43.5	59.2	11.3	17.2	1

The detection performance of the resampled data was very similar to that of the full data, indicating the number of acquired wavelengths can be decreased without detriment to the detection rate. Surprisingly, the number of false positives appeared to decrease with the resampling, suggesting using a fewer number of wavelengths may be a superior approach for the interactance measurements.

2.7 Effect of sample age on nematode detection rate

There appeared to be an effect of sample age and handling on the how well the algorithms performed. Groups A and B, the older fillets, were combined into Group 1 and Groups C and D, the fresher fillets, were combined into Group 2. The older group experienced a markedly lower detection rate. However, it is not possible to separate how much of the difference is due to the age of the samples and how much is caused by the handling of the samples after they have been filleted. Interestingly, the number of false positive also decreased in the older group. While a few more of the deeper nematodes appear to be detected in the fresher fillets, shown Figures 14 and 15, the effect did not appear significant and the low number of nematodes makes it difficult to draw any definitive conclusions.

Table 3   Statistics for the two different sample groups

Method	Group 1 **Detection rate (%)**	Group 2 **Detection rate (%)**	Group 1 Average False Positive Rate	Group 2 Average False Positive Rate
LDA	34.4	45.9	5.5	7.7
LDA+SVM	28.1	43.9	2.9	3.6

Figure 14   Nematode distribution and detection rate as a function of depth for the LDA classification for a) Group 1 and b) Group 2. Red color indicates nematodes detected, blue color indicates nematodes not detected. The total height of each bar corresponds to the total number of nematodes at each depth.
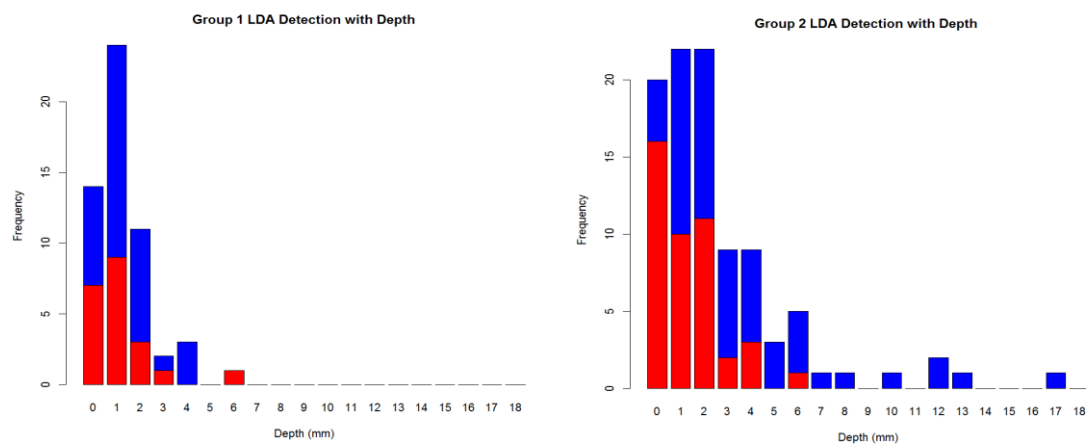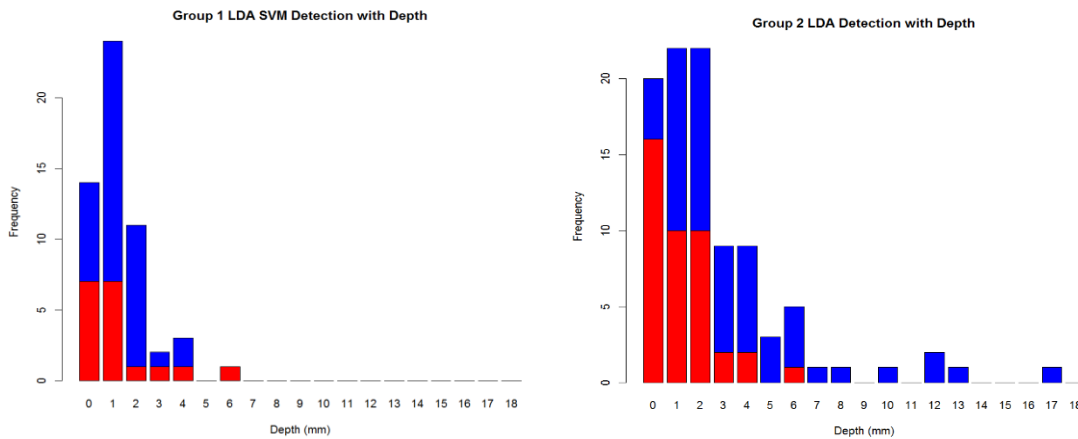
Figure 15   Nematode distribution and detection rate as a function of depth for the LDA SVM classification for a) Group 1 and b) Group 2. Red color indicates nematodes detected, blue color indicates nematodes not detected. The total height of each bar corresponds to the total number of nematodes at each depth.

2.8   Blood detection

Figure 16 shows an example of estimation of blood concentration based on constrained spectral unmixing of hyperspectral images. The color image in a) and the blood concentration image in b) are based on diffuse reflectance imaging, as described in (Skjelvareid et al. 2017), while the image in c) is based on interactance imaging. The two blood concentration images may appear quite similar, but however differ in a number of ways:

- The interactance image appears "smoother" in the loin and belly, which is closer to the distribution of blood that is expected in these parts. The rough texture of the diffuse reflectance image may be due to surface scattering effects.

- In the interactance image, it is possible to "see through" the black lining and detect the blood veins underneath. The small blood spots along the center line are also more clearly seen. This illustrates that diffuse reflectance imaging is basically a surface technique, while interactance imaging can be used to "see deeper".
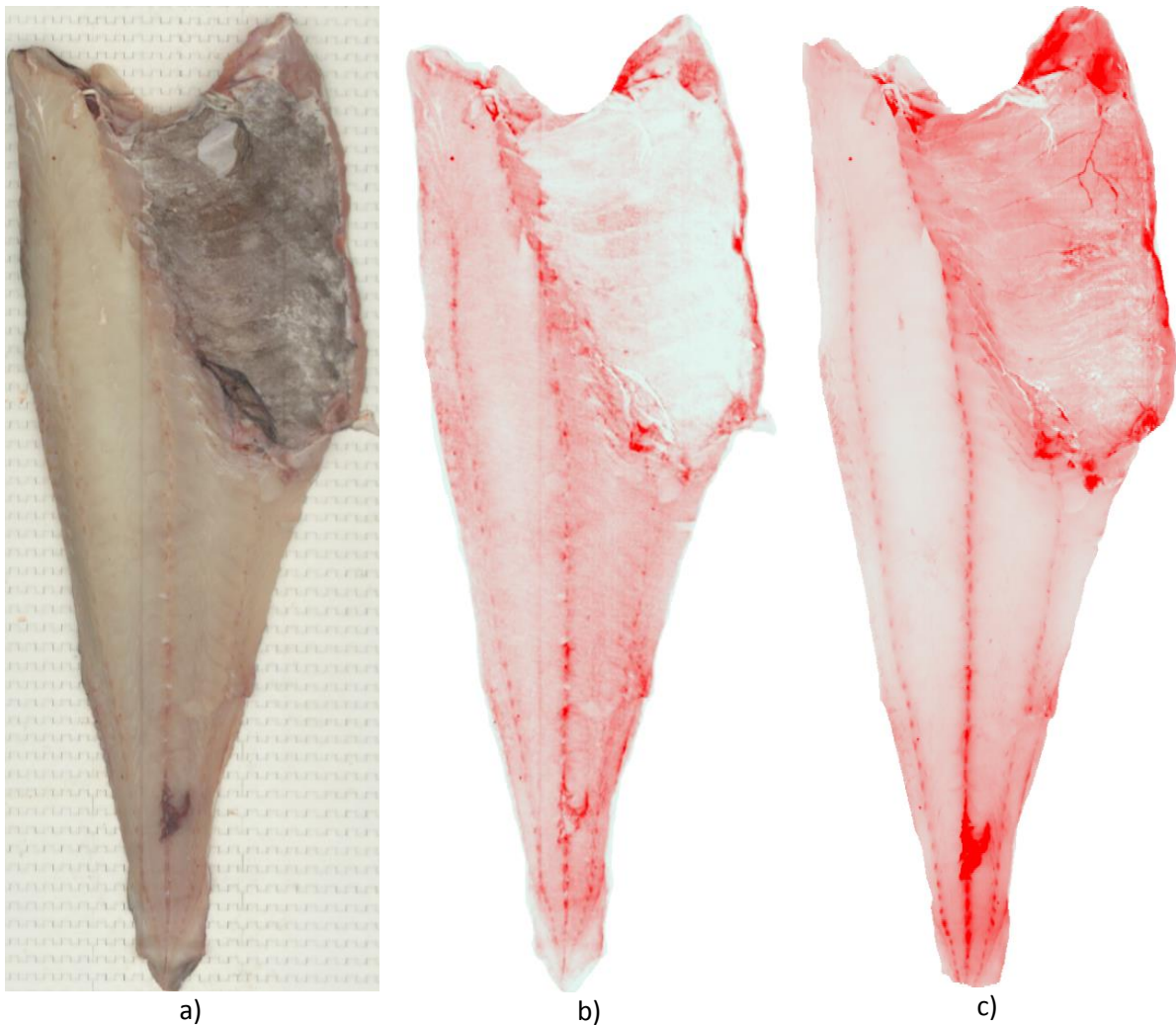
Figure 16   *Fillet analyzed for blood based on hyperspectral data. a) Calibrated color image based on diffuse reflectance hyperspectral imaging. b) Estimated blood concentration based on diffuse reflectance hyperspectral imaging. c) Estimated blood concentration based on interactance hyperspectral imaging.*

2.9   Discussion – nematode detection in interactance images

In the joint test experiment described here, the detection rate achieved by the best performing classifiers was approximately 40 %. This is lower than that reported in earlier work using a similar interactance setup (Agnar H. Sivertsen et al. 2012), where a 50.7 % detection rate was a achieved if 60 % of fillets were allowed to have one or more false positives. There are several expected causes for the disparity between the studies. One expected reason is that some of the fillets included in the experiment here were several days old and subjected to extensive handling due to multiple imaging sessions. Because scattering increases as the fillets age, this is likely to have an adverse effect on detection rate as it will impact both how deeply nematodes can be detected and the spectra from image locations with nematodes will contain a larger spectral contribution from the surrounding muscle. The "group 2 detection rate" of approximately 45 % for the fresher fillets, given in section 2.7, is closer to that reported by Sivertsen et al. Another possible explanation for the disparity is that in the trial by Sivertsen et al., both training and validation data was recorded by placing the hyperspectral imager at-line in the filleting facility. With this approach, the training and validation are more

consistent, and the fillets are not affected by storage or handling. In the experiments described here, the fillets in both training and validation sets were stored for several days (and an unequal number of days), and some fillets were handled extensively.

Another potential reason why the detection performance in the current study decreased compared to the earlier study is that while the shorter distance between the illumination and measurement lines improves signal to noise, the depth of measurement also decreases. Therefore, some nematodes that may have been detected by the old light line system may have been too deeply buried to be measured by the current setup. The relationship between light line distance and the depth of measurement has not yet been quantified in cod.

Finally, although the number of nematodes in the test described here was fairly high (199), a majority of these were found in a small number of fillets - the 5 fillets with the highest number of nematodes contained 101 nematodes in total. This means that the statistics are dominated by a small number of fillet samples and may therefore not be very reliable. Furthermore, many of the fillets have other quality defects that may impact the quality of the detection algorithms. Given the small sample set available, determining whether and how much other types of quality defects impact the nematode detection rate is not possible here and would need to be the subject of future work.

The statistics showing detection rate as a function of nematode depth and size indicates that the detection rate is strongly dependent on nematode depth (almost no nematodes deeper than 4 mm detected), but less dependent on nematode size (some nematodes as small as 2 mm in diameter were detected). However, making definitive conclusions is difficult because of the small available sample set of large nematodes and nematode size and depth are correlated - the larger nematodes are predominantly *Pseudoterranova Decipiens,* which tend to be buried more deeply in the flesh.

3 Ultrasound – methods and results

3.1 Methods and materials

3.1.1 Ultrasound instrument

A Logiq Book XP Vet ultrasound instrument with an 8 MHz linear probe was used for the experiments. The equipment is shown in Figure 17. Images were acquired with 60 dB dynamic range and neutral time gain compensation (TGC). Selected screenshots from the imaging were exported as JPEG files.

3.1.2 Cod fillets with nematodes

A single fillet ("A09") was selected from the experiment conducted in November 2016, described in section 2.4.1. This fillet was chosen because it was the only one with clearly visible, large and darkly colored nematodes (most probably *Pseudoterranova decipiens)*, which was considered a "best case" for detection. Since detection of these nematodes proved to be very challenging, the experiment was not extended to include additional fillets. The fillet and the 5 nematodes which were imaged are shown in Figure 18.

3.2 Results and discussion

Results from the nematodes that were imaged are shown in Figure 19. The images represent a «slice» through the fillet, with the fillet surface in the top of the image and the table surface in the bottom, visible as a bright line. The images show that the nematodes seem to reflect some amount of ultrasound energy, making them slightly brighter than the muscle tissue background. However, the curled-up shape of the nematode cannot be recognized in the image, and there are other structures in the muscle tissue that yield similar responses. The images also display some amount of "speckle", a type of background noise visible in all ultrasound images of biological tissue. In sum, these effects make it very challenging to recognize nematodes in the images without knowing their position beforehand. During imaging with the handheld probe, capturing the nematode response took several attempts, even though the nematode was clearly visible to the naked eye and the probe was placed directly above the nematode.

If ultrasound imaging were to be used for nematode detection on an industrial scale, it would not be possible to use the handheld instrument used here, and the results are therefore not completely representative for what could be achieved using a more customized imaging solution. However, the physical properties of the nematodes and the fish muscle tissue would to a large extent be the same, and we therefore believe that robust detection of nematodes with a low number of false positives will be very challenging, regardless of which ultrasound system is used.

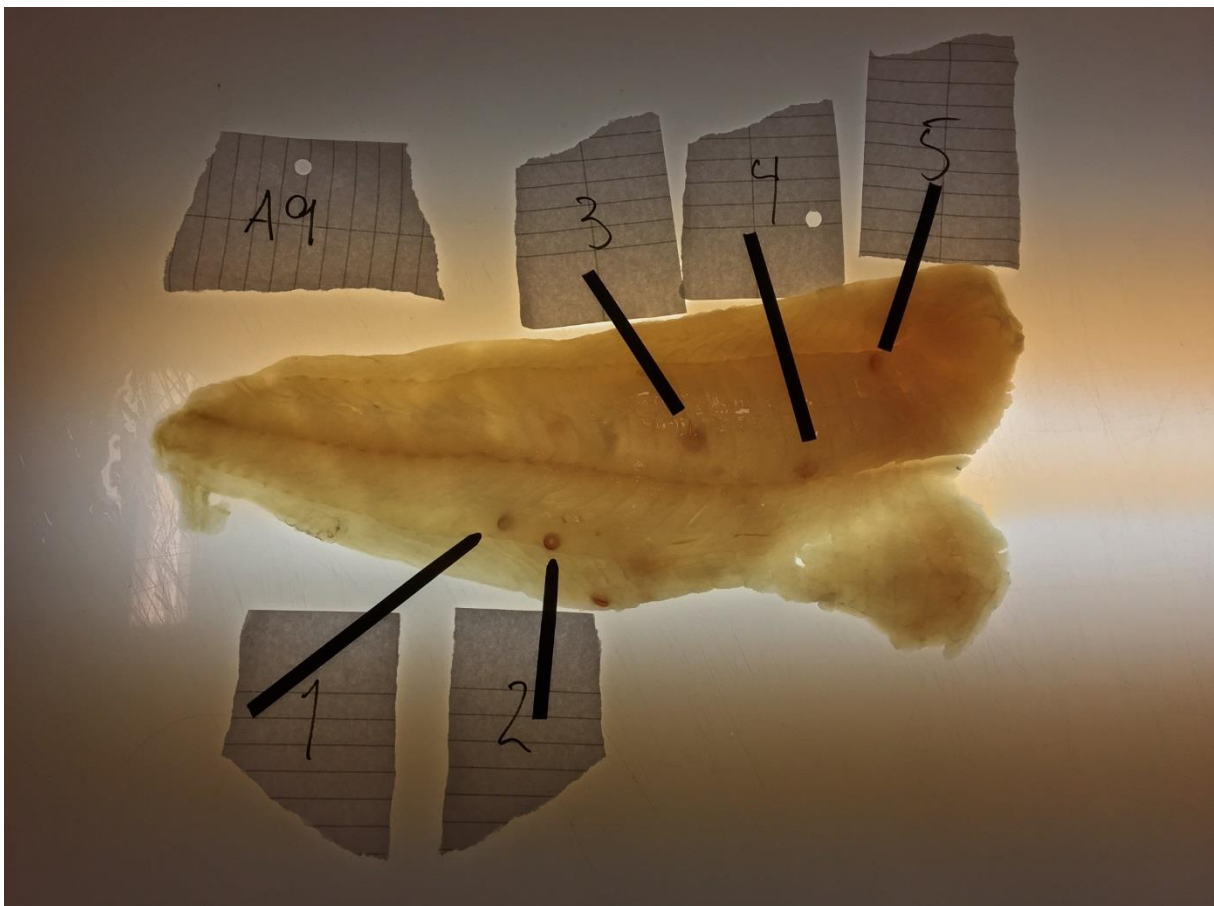*Figure 17   Ultrasound instrument and probe used in experiments.*

Figure 18   Fillet A9 with indication of the five nematodes which were imaged using ultrasound. The fillet is placed on a white plastic plate, backlit by a fluorescent light.
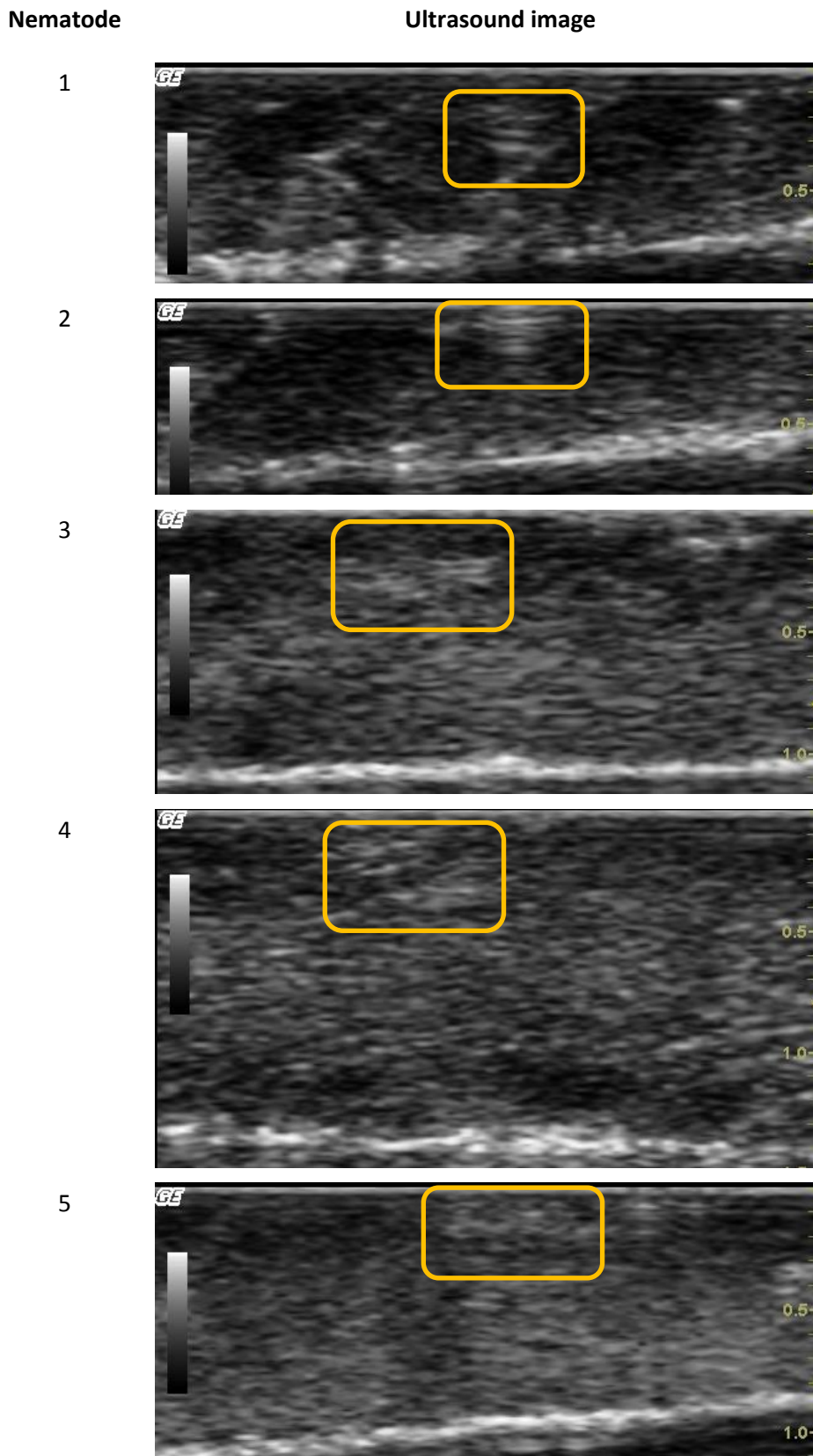
Figure 19   Ultrasound images taken with the ultrasound placed directly above each nematode. The vertical axis corresponds to depth inside the fillet (cm). Image features which are assumed to correspond to nematodes are indicated with orange rectangles.

4 Dual-energy X-ray CT – methods and results

4.1.1 Background

X-ray imaging is performed by illuminating a sample with energy in the X-ray and observing the attenuation. X-ray attenuation is controlled by sample density and atomic number:

$$I = I_0 \exp(-\mu \rho x)$$

Where *I* is the measured intensity, I_0 is the initial intensity of the x-ray beam, ρ is the density and *x* is the path length. For normal X-ray images, the contributions of density and atomic number to signal intensity cannot be separated. Dual X-ray imaging makes measurements at two different X-ray energies. At lower energy, the attenuation is dominated by the photoelectric effect, which is mainly affected by atomic number. At higher energy, attenuation is dominated by Compton scattering, which is more strongly controlled by density. When the two measurements are analysed together, contrast is improved. If the measurement is performed with samples of known density and atomic number, the images of the sample can be calibrated to be density and atomic number maps.

4.1.2 X-ray CT equipment

A siemens Somatom definition flash was used to perform the measurements. Images were 512 by 512 pixels

4.1.3 Cod fillets with nematodes

X-ray CT measurements were performed on six different fillets from the November 2016 measurement. Three of the filets were in the frozen state (A02, A05, A06) and three of the filets were in the thawed state (A03, A09, A10). It is not anticipated that there will be a significant difference in results between the fresh and thawed states. Most fillets contained anisakis nematodes with the exception of A09, which contained several pseudoterranova.

4.2 Results and discussion

Detection of nematodes was possible for both the frozen and thawed states; it was expected that it may be easier to detect nematodes in the frozen samples due to the slightly lower density of water in the frozen state, but no obvious difference in image quality between the thawed and frozen samples was noted. This finding suggests the method has potential for screening whole fish in the frozen state before they reach the filleting process.
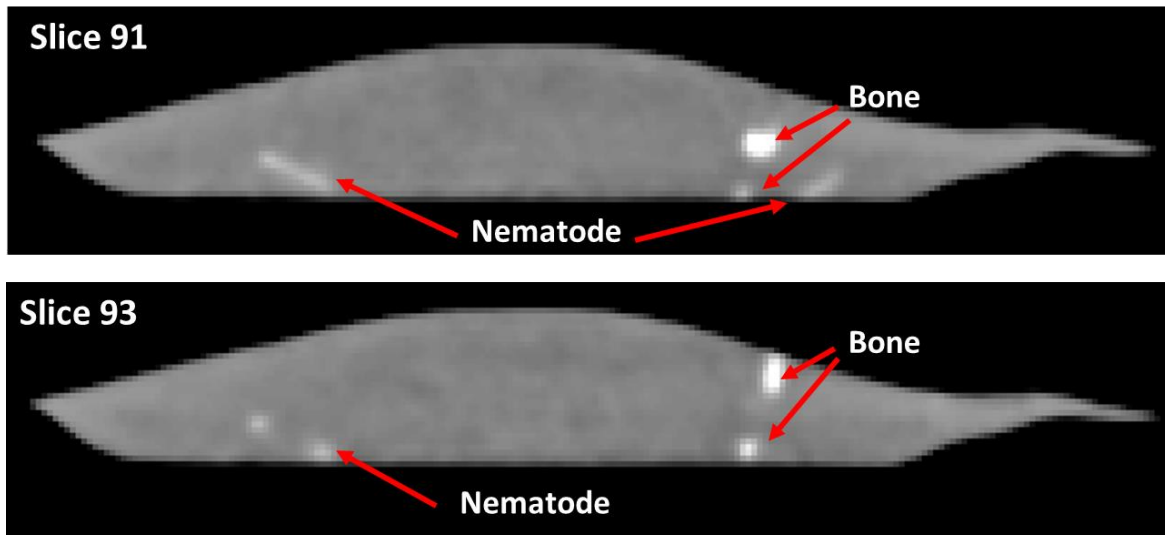
Figure 20   Slices from a 3D reconstruction of thawed cod filet A09

Figure 20 shows slices from a 3D CT image of thawed cod fillet A09. Nematodes can clearly be distinguished from the surrounding tissue. By stepping through images, the curled shape of the nematodes can also be seen. Bone appears distinguishable from nematode due to higher density, however classification of the two was not attempted so the robustness of the identification is unknown.

4.3   Summary

Dual energy X-ray CT appears to be an effective way to detect nematodes within fish fillets, particularly those too deeply imbedded to be detected with other methods. However, the method has several drawbacks. Scanning time per filet is too slow to be able to scan at a rate compatible with industrial production. Equipment cost is also prohibitively high for industrial scale application. Therefore, the CT modality of x-ray imaging is not feasible for industrial use and simpler X-ray imaging modalities that are faster and cheaper need to be evaluated.

5 Dual-energy X-ray planar imaging – methods and results

5.1.1 Planar X-ray equipment

The planar imaging system used was a Canon CXDI wireless producing image of 2711 by 1333 pixels and a 0.125 mm pixel size. While not strictly a true dual energy system, the system has the capability to measure at energies ranging from 40 keV to 150 keV, allowing a dual energy contrast image to later be created in post-processing from two measurements at different energies.

5.1.2 Cod fillets with nematodes

Sample A01 from the May 2017 testing was used to evaluate x-ray planar imaging for nematode detection. The fillet contained both anisakis and pseudoterranova species of nematodes. The sample was in the thawed state, having previously been frozen at -30 C.

5.2 Results and discussion

Dual energy x-ray CT images were measured at energies of 140 keV and 80 keV. However, due to differences in the detectors in the equipment, images above 50 keV saturated the detectors due to the low attenuation of the fillets. This made acquisition of images at two different energy levels not possible using the available system. Single energy images were measured at the lower end of the energy spectrum of the system to see whether nematodes could be detected using those alone.
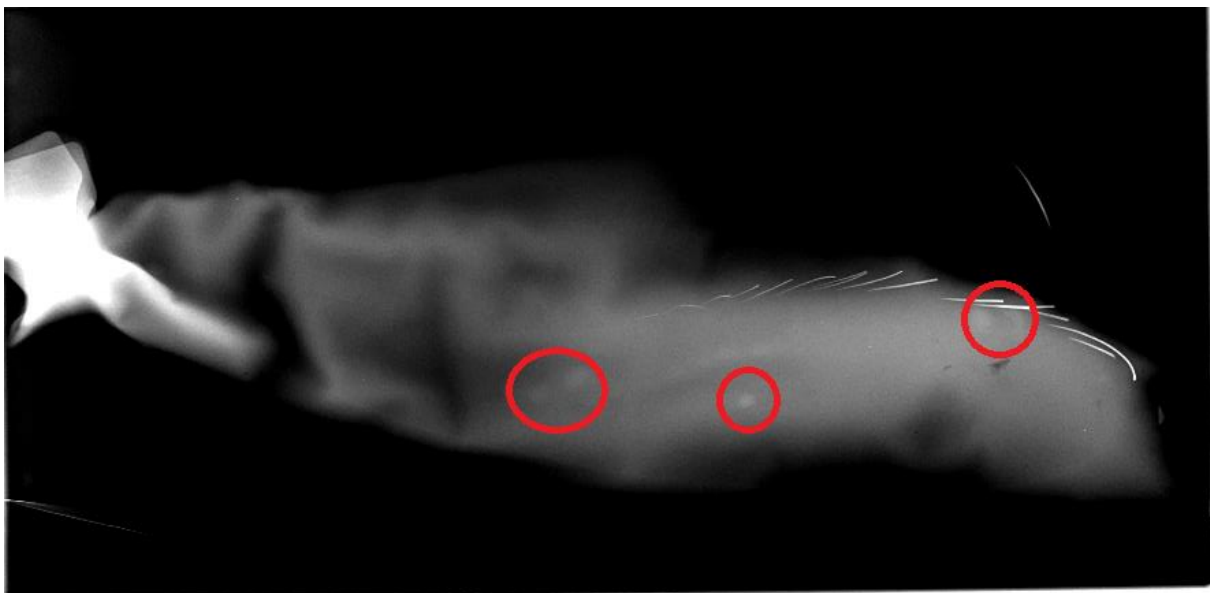

Figure 21   Planar X-Ray image taken at 40 keV with a 20 ms exposure

The best image was acquired using 40 keV with a 20 ms exposure, shown Figure 21. While there is no detail in the thinner belly part of the fillet due to detector saturation, there are several white spots in the loin of the fish, indicating locations of slightly higher attenuation. Several of these spots are in similar locations as to where nematodes were found during dissection. Furthermore, it appears that two such similar spots were observed in the same location by SINTEF. This suggests that detection of nematodes using a single energy image alone may now be possible due to improvements in x-ray imaging systems since previous studies were undertaken. However, results need to be treated with

caution as there is not an excellent correspondence between the planar X-ray and dissection results. Furthermore, due to the low contrast between the tissue and possible nematodes automation of image analysis may be a challenge.

5.3   Summary

The results indicate that X-ray planar imaging may be suitable for detection of nematodes, particularly those located in the loin of the fillet, but results are not definitive. Given the time limitations, the study is not considered exhaustive and further studies would be needed to extensively evaluate the suitability of planar X-ray for nematode detection. A limitation of the study is that the equipment used has been designed to measure hard tissue, such as bone. Therefore, the available acquisition parameters may not be ideal for a soft tissue sample such as a fish fillet. A suggestion was made to evaluate the technique using a mammogram system, which are optimized for soft tissue measurement.

6 System cost evaluation

The purpose of this section is to give a rough idea about the material costs for a complete system for detection of embedded defects based on interactance hyperspectral imaging. Although CT X-ray, planar X-ray and ultrasound are also discussed in this report, experiments with these techniques were preliminary in nature, and we have very limited information about how these could be implemented in an industrial setting. Cost evaluation for these techniques is therefore not included here.

Illumination

The fiberoptic light lines used for interactance imaging in this report was manufactured by Fiberoptics Technology Incorporated[1], with custom made lenses made by Optec[2]. To avoid overheating of the fiberoptics by the halogen lamps, 1000 nm shortpass filters made by Illumination Technologies, Inc.[3] were used. If only production costs are considered (not design/engineering), the total price for two light lines with power supplies and shortpass filters was € 20 800. This price would probably be considerably lower for mass production. The illumination also includes lamp holders with active cooling, custom made by Marel, but the material cost for these will not be included here.

However, it may be possible to make a simpler illumination system based on LEDs. For example, Nofima has purchased UV LED line lights from Metaphase Lighting Technologies[4] at a price of € 4400 for two light lines. Similar products[5] are available with white LEDs covering the visible range (approx. 450-700 nm) and 850 nm. It is also possible to order custom-made line lights with combinations of different LED types.

Hyperspectral camera

The VNIR1024 hyperspectral camera used in this report cost approximately € 50 000. However, this is a scientific-grade, high-end system, with a higher spectral resolution than what is needed for the applications discussed here. According to personal communication with Trond Løke at NEO, they will be releasing a new hyperspectral camera for industrial use in 2018, with an approximate price of € 20 000. Other hyperspectral cameras with similar specifications, such as the SpecIm FX10[6], have similar prices (we were not able to get specific prices during writing of the report).

Depending on the requirements for spectral resolution and spectral range, it may also be possible to use a number of filter-based multispectral cameras, such as those manufactured by IMEC[7] or Chromasens[8]. Again, we do not have specific prices, but these cameras are simpler than full hyperspectral cameras and are assumed to have a lower price. Here we assume a very approximate price estimate of € 5 000.

---

[1] http://www.fiberopticstech.com

[2] http://www.optec.eu

[3] https://illuminationtech.com/

[4] https://www.metaphase-tech.com/page/home

[5] https://www.metaphase-tech.com/line_lights_line_scan/metabright_line_light

[6] http://www.specim.fi/fx/

[7] https://www.imec-int.com/en/hyperspectral-imaging

[8] https://www.chromasens.de/en/product/multi-spectral-camera-truepixa-compact-12-channel-90dpi

Image acquisition and processing computer

Nofima has recently purchased a new computer with a graphics card, to test on-line acquisition processing of hyperspectral data using GPU processing. The computer cost approximately € 6 000 including the graphics card.

However, there is on-going development on specialized hardware for processing of hyperspectral data. At the Conference on Hyperspectral Imaging in Industry in 2017 (CHII, Graz, Austria), the company Perception Park presented a GPU-based hyperspectral processing unit approximately the size of a credit card (but approx. 1 cm thick), designed for onboard-processing in UAVs. With mass production, units like these should be significantly cheaper than the computer described above. No price was given at the conference, but we will assume a price of approximately €3 000.

Total system cost

Table 4   Estimated total system cost for hyperspectral imaging.

Component	Cost (current system or similar)	Possible low-cost alternative
Illumination	€20 800	€4 400 (LED system)
Camera	€20 000	€5 000 (filter-based multispectral)
Image acquisition/processing	€6 000	€3 000 (specialized GPU unit)
Total	€46 800	€12 400

Note that these are only the costs for the main components of the system. The components would have to be mounted into custom-made cabinets, with additional electrical components, possibly cooling, etc. The system would also have to be integrated with conveyor belts, encoders, sorting machines etc. Engineering and software development will also represent significant initial costs.

7 Conclusions

Hyperspectral Imaging:
- Improvements to the illumination setup of the interactance imaging system had been made since the previous study in 2012. In the new setup, the light line had been made more focussed, allowing illumination closer to the measurement line and improving signal to noise. The depth of measurements decrease with shorter distance between illumination and measurement line.
- For the best two classification methods, the average nematode detection rates were 41.4% and 37.7%, with average false positive rates of 6.5 and 3.2 per fillet. Using a simplified dataset with 14 spectral channels, the best two classification methods yielded a detection rate of 41.3% and 43.5% with average false positive rates of 4.3 and 17.2 per fillet.
- Reliable detection of nematodes more than 3 to 4 mm under the imaged surface does not appear possible to due attenuation and scattering effects.
- A reliable relationship between size and detection rate cannot be determined with the data set available. There is a strong correlation between nematode size and depth (i.e., the larger pseudoterranova nematodes tend to be deeply buried in the fillets) and there is not enough variation in the data to allow the two effects to be deconvoluted.
- Sample age and handling appears to have a negative impact on detection rate. Measurements here were performed in the lab on cod that had been filleted from 3 to 6 days prior. Detection rate for the older fillets was noticeably worse than for the fresher fillets. Overall performance was worse than the 2012 study, where measurements were made on freshly filleted samples.
- Imaging of blood using an interactance setup gives smoother images than with the diffuse reflectance image acquisition mode and allows blood to be detected underneath the black lining
- The main source of false positives in the images arose from blood and edge effects. It is expected that with further work, these types of false positives can be solved, which leaves a false positive rate of approximately 1-2 false positives per fillet

Ultrasound: In the pulse-echo ultrasound images acquired in this project, there was generally poor contrast between nematodes and fish muscle tissue. This, combined with image "noise" from other structures in the muscle tissue, makes automatic nematode detection in ultrasound images very challenging. Ultrasound imaging is therefore not considered a suitable technology for detection of nematodes in fish fillets.

X-Ray Imaging: Preliminary results using dual energy X-ray CT capability are promising for detection of nematodes but are not feasible for industrial scale implementation. Imaging of nematodes in the loin of the fish appears potentially possible using planar X-ray equipment, but further testing is required to determine whether enough contrast can be produced to reliably distinguish nematode from muscle.

Best candidate for detection of embedded nematodes: Given that no deeply embedded nematodes were detected by interactance imaging, and that ultrasound appears to yield too low contrast between nematodes and fish muscle, planar X-ray imaging seems to be the most promising technique for deeply embedded nematodes. However, the experiments conducted on planar X-ray were limited to a single fillet, and the results were inconclusive. Further research on both instrumental parameters (X-ray energy, sensor parameters etc.) and image analysis is needed before the technique is ready for industrial prototyping.

Future work

In an eventual follow-up project, trials should be performed at-line in industry, if possible. This is to ensure that the spectra measured from the fillets are representative of the spectra that would be encountered in an industrial implementation. While not exhaustive nor conclusive, the results between the two measured groups in the joint test indicates detection ability decreases with fillet age. This suggests results obtained in a lab setting will be more pessimistic than results obtained on site.

The effect of other quality defects in the fish on the detection rate should be investigated. In particular, blood in the fillets may have a negative impact on the ability to distinguish nematodes from the surrounding tissue.

The experiments on X-ray imaging described in this report were performed in a very limited in time, since they made use of hospital X-ray equipment. Further experiments on should be performed in a lab setting, with access to the X-ray equipment over several days. This will ensure that there is enough time to optimize the imaging parameters. Furthermore, the equipment used was some years old and newer equipment with better sensors exist, which may provide more sensitivity to aid in distinguishing nematode from muscle.

8 References

Levsen, A., B.T. Lunestad & B. Berland (2005). Low Detection Efficiency of Candling as a Commonly Recommended Inspection Method for Nematode Larvae in the Flesh of Pelagic Fish. *Journal of Food Protection,* **4**, International Association for Food Protection: pp. 660–884. http://www.ingentaconnect.com/content/iafp/jfp/2005/00000068/00000004/art00026.

Pétursson, J. (1991). Optical Spectra of Fish Flesh and Quality Defects in Fish. In *Fish Quality Control by Computer Vision*, edited by Pau, L.F. & R. Olafsson, pp. 45–69. Marcel Dekker, Inc.

Sivertsen, A.H.., K. Heia, K. Hindberg & F. Godtliebsen (2012). Automatic Nematode Detection in Cod Fillets (Gadus Morhua L.) by Hyperspectral Imaging. *Journal of Food Engineering*, **111**:4, pp. 675–81. http://www.sciencedirect.com/science/article/pii/S0260877412001161.

Sivertsen, A.H, K. Heia, S.K. Stormo, E. Elvevoll & H. Nilsen (2011). Automatic Nematode Detection in Cod Fillets (Gadus Morhua) by Transillumination Hyperspectral Imaging. *Journal of Food Science*, **76**:1, pp. 77–83. doi:10.1111/j.1750-3841.2010.01928.x.

Skjelvareid, M.H., K. Heia, S.H. Olsen & S.K. Stormo (2017). Detection of Blood in Fish Muscle by Constrained Spectral Unmixing of Hyperspectral Images. *Journal of Food Engineering.* doi:10.1016/j.jfoodeng.2017.05.029.

9 Appendix

9.1 PCA modelling for nematode detection in interactance images

9.1.1 Mean spectra for different pre-processing options

The mean spectra for each class of object (nematode, belly etc.) and for each type of pre-processing applied are shown in Figure 22. Note that the spectra show light intensity (corresponding to camera output) and not light absorption. In the spectra without pre-processing, it is seen that below 600-650 nm, the center line and the nematodes absorb more light than the three muscle classes. The area normalization and SNV are seen have approximately the same effect on the spectra, with the exception that SNV spectra are centered around 0. The main spectral differences are still below 600-650 nm Finally, the derivative pre-processing mainly shows spectral differences in a relatively narrow range around 550-650 nm.

9.1.2 PCA coefficients for different pre-processing options

To better understand the PCA models for the different pre-processing options, the first three components were plotted together with the mean vectors used for centering the spectra (a "centered" version of PCA was used). These plots are shown in Figure 23.

It is interesting to note that the PCA coefficients for the raw, area normalized and SNV transformed spectra all show approximately the same spectral features. However, PC1 for the raw spectra is almost completely flat, indicating that a lot of the variation in the data set is due to baseline shifts between the spectra. With area normalization and SNV transformation, this variation is no longer present, resulting in PC1 for these datasets being very similar to PC2 for the raw spectra.
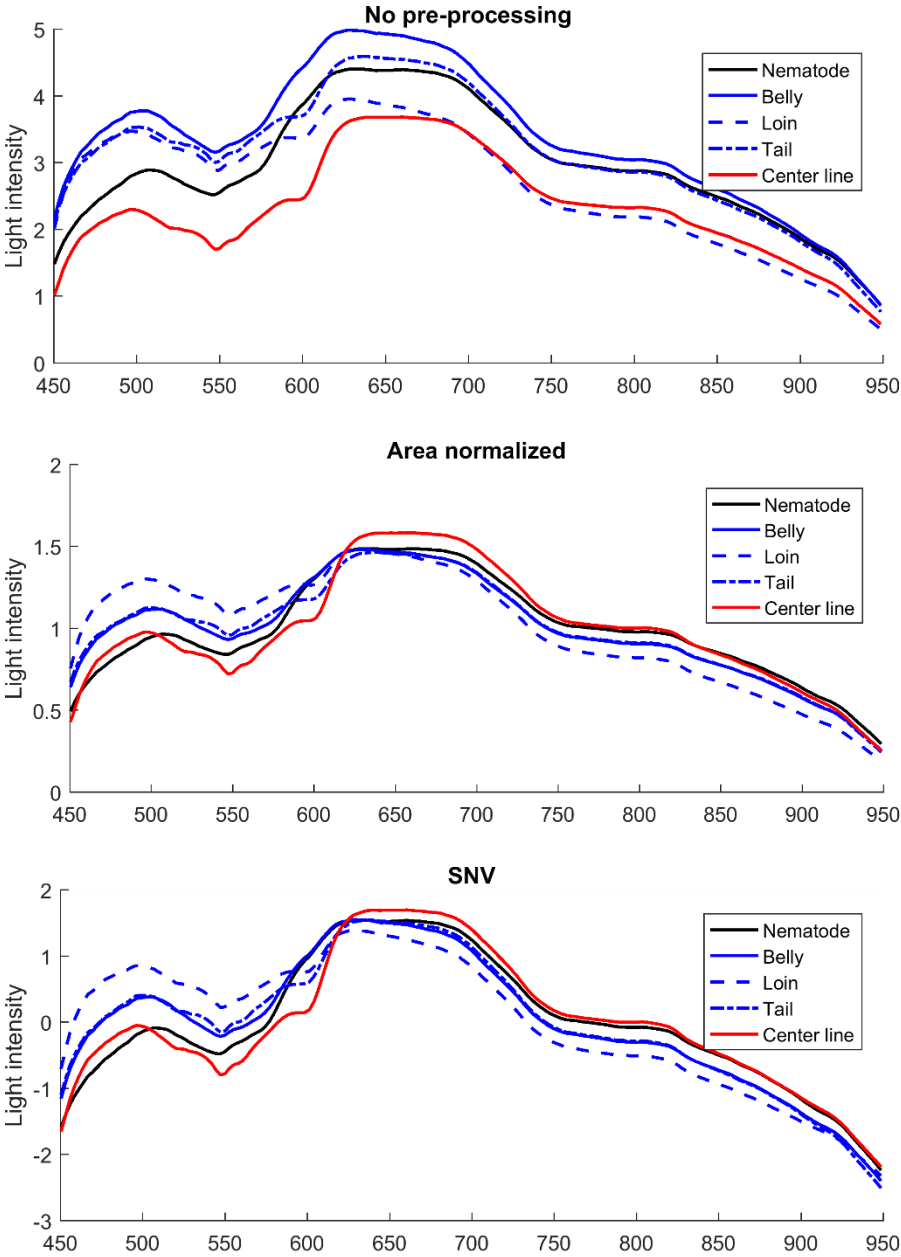
For all pre-processing methods, the PCA coefficients show that the sharpest and most characteristic spectral features are below approx. 650 nm.

9.1.3 Scatter plots for different object classes

Figure 24 shows scatter plots for all training data used for the PCA models, for different pre-processing options. For "no pro-preprocessing", PC2 and PC3 is plotted, since PC1 corresponds mainly to baseline shifts. For the other pre-processing options, PC1 and PC2 is plotted. In addition to the scatter plots, ellipses fitted to each class is shown, to better visualize the distribution where the scatter plots are overlapping. The ellipses correspond to 2-D 95% confidence intervals, calculated assuming a Gaussian distribution[9]. The plots show that the nematode class (blue) is different from muscle and centre line classes, but that there is also a significant degree of overlap. Figure 25 shows a similar plot for data collected from the high-pass filtered PCA images. The muscle and center line classes are more or less collapsed into overlapping classes, while the nematode class has less overlap. This is due to the small size of the nematodes, making them "stand out" in the high-pass filtered images. However, there is still a significant degree of overlap, indicating that accurate nematode detection with low number of false positives is non-trivial. Note also that the scatter plots shown here only contain part of the

---

[9] https://se.mathworks.com/matlabcentral/fileexchange/4705-error-ellipse

information from PCA analysis (only two PCs), and that information in higher component numbers may also help in classifying nematodes.
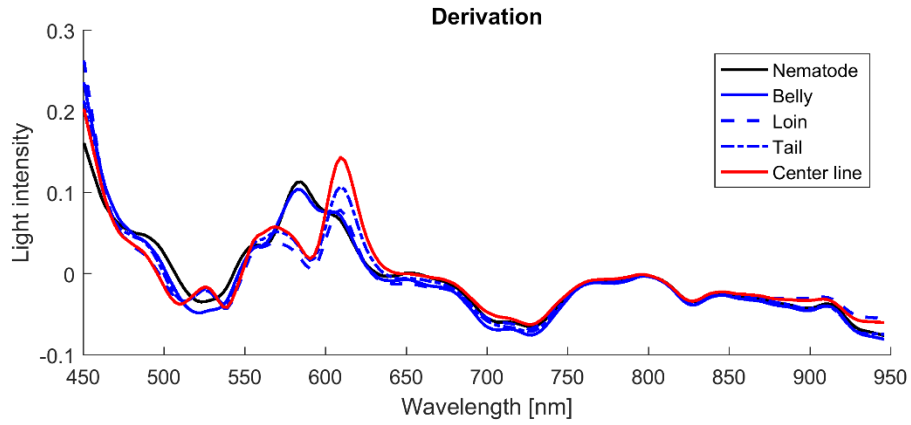
Figure 22: Mean spectra of the five classes used in PCA modelling, for raw data and three different pre-processing methods..
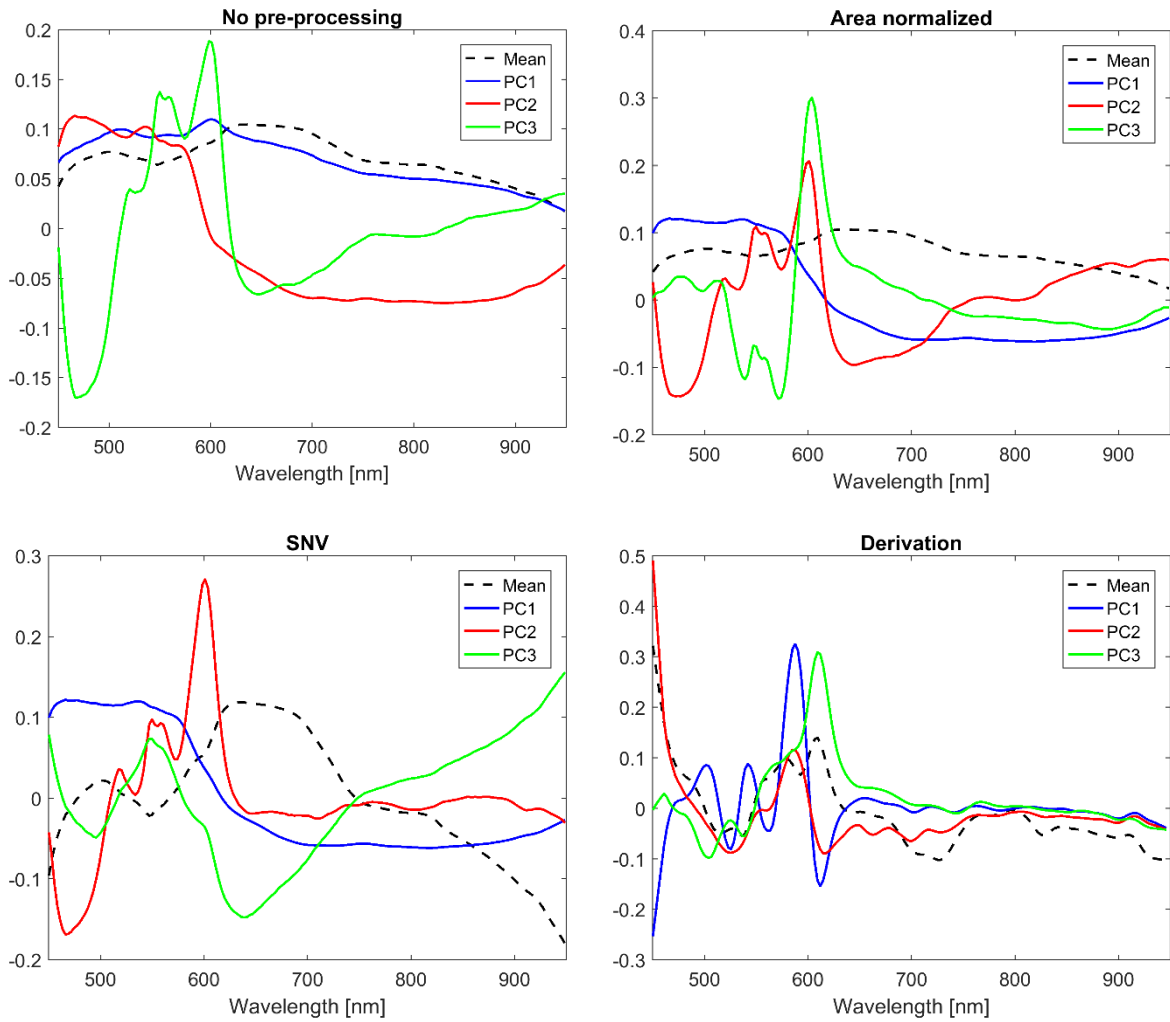

Figure 23 PCA coefficients for different pre-processing options. Note that the "mean" vector, used for centering prior to PCA, was scaled as a unit vector (same as for principal components) for easier comparison.
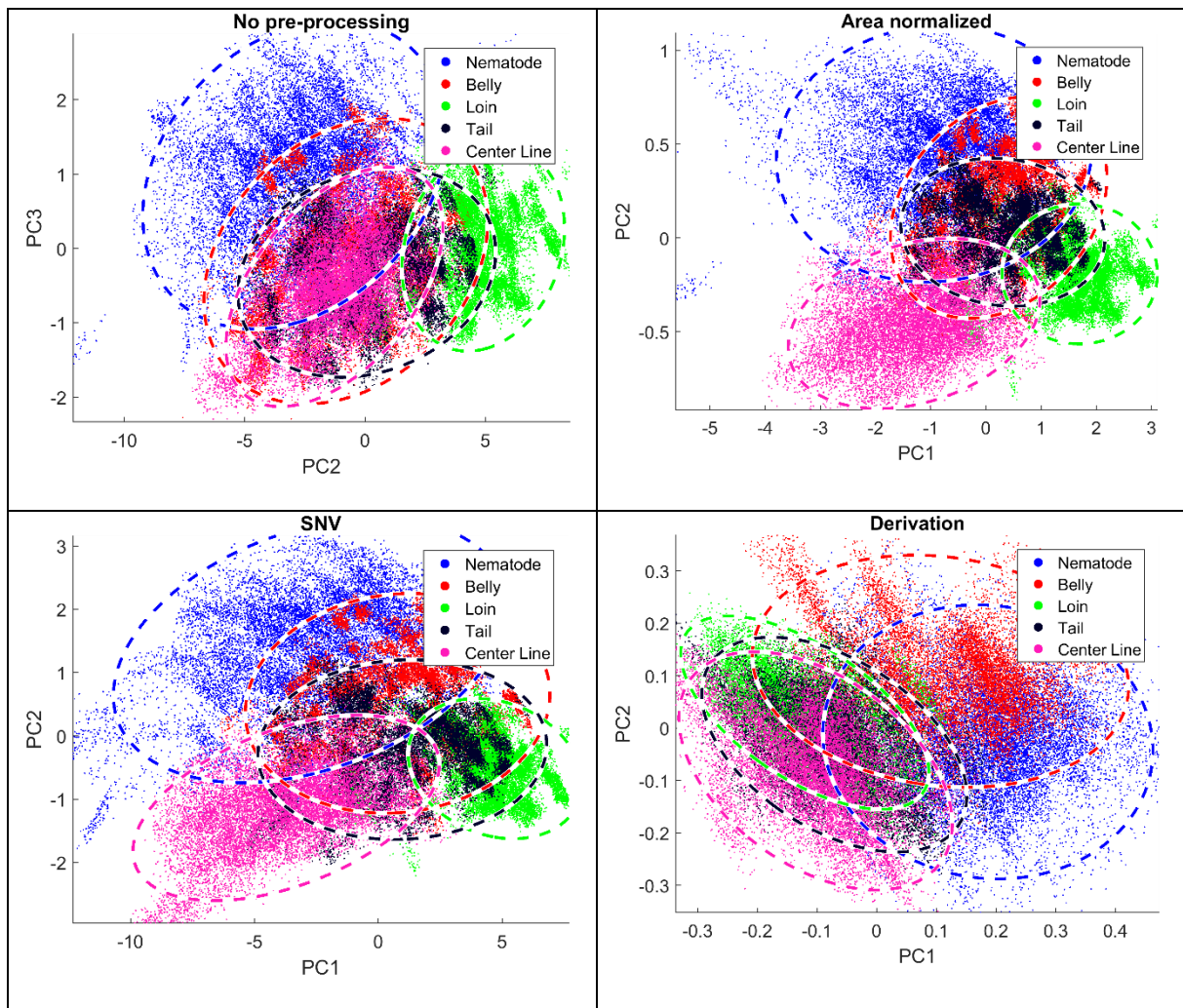
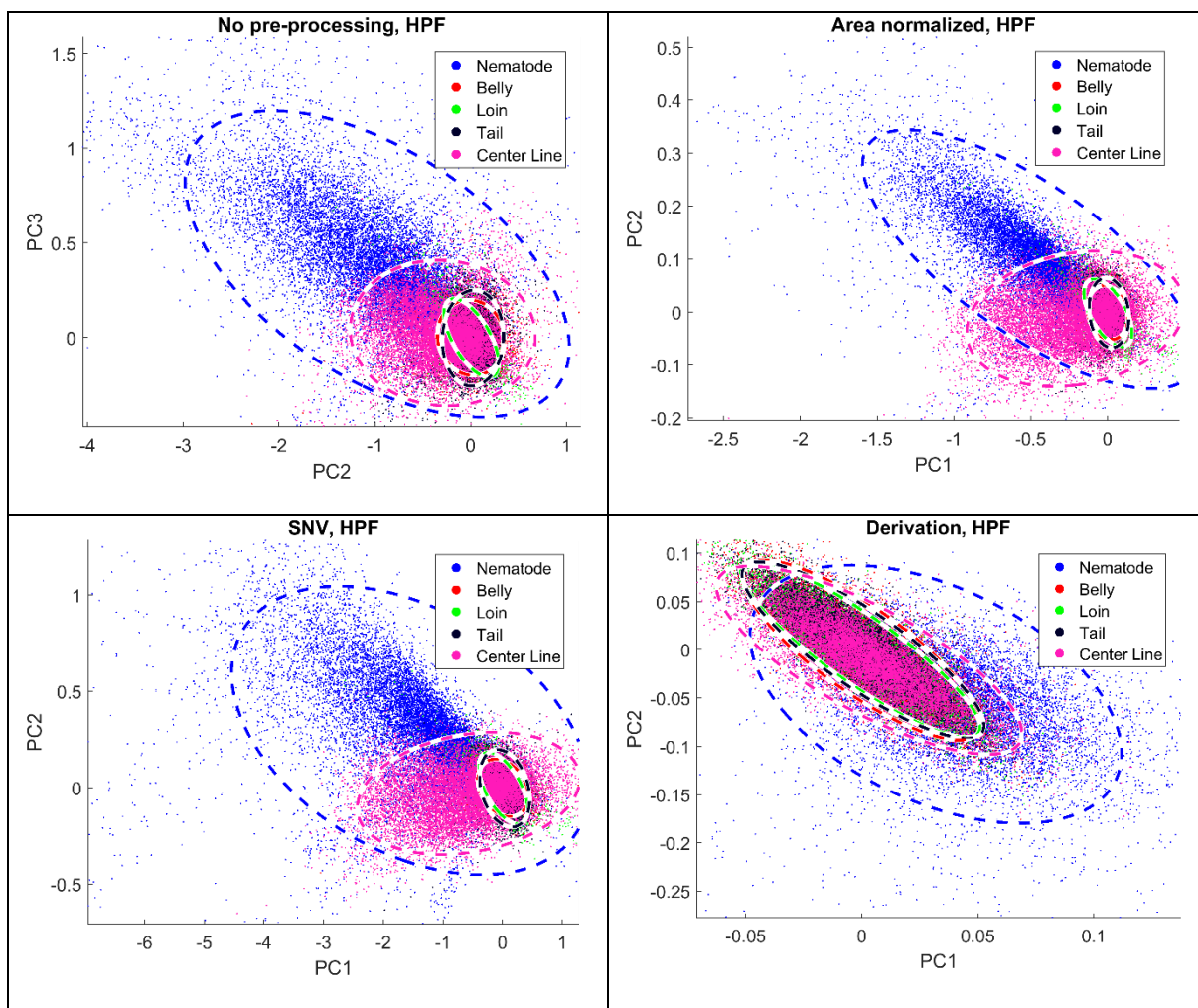*Figure 24 Scatter plots for different types of pre-processing.*

Figure 25   Scatter plots for high-pass filtered PCA images

9.2 Preliminary test using SWIR hyperspectral camera

During a short period in the autumn of 2016, Nofima had access to a SWIR-384[10] hyperspectral camera from NEO. This camera is similar to the VNIR-1024 camera used for hyperspectral imaging in the main part of this report, but it operates at longer wavelengths (1000-2500 nm, the short wave infrared range) and has a lower spatial resolution (384 pixels across-track). This section describes some preliminary experiments which were done to evaluate the potential of this camera for nematode detection. The experiments were also meant to serve as a guideline for Sintef, to enable them to choose the best wavelengths for their transmission mode measurements (presented in a separate report).

In biological tissue such as fish muscle, scattering causes the light to lose its direction (it becomes a diffuse light field) and also limits the penetration depth of the light in the tissue. Scattering generally decreases with increasing wavelength, and by imaging at long-wavelengths, one can expect the images to be less affected by scattering than at shorter wavelengths. However, absorption of light by water generally increases with wavelength from approximately 500 nm and upwards, and to obtain a low-scatter image with enough light, it is necessary to use a wavelength range which balances the effects of scattering and absorption.

Previous studies (Pétursson 1991) have shown that in the wavelength range around 1300 nm, the scattering in fish flesh is relatively low, while scattering by nematodes is higher. This could yield a contrast between fish muscle and nematodes in a transmission mode image. At this wavelength range, the absorption due to water is also still low enough to allow some light to penetrate through a fish muscle sample.

A preliminary test was performed using fish from the experiment described in Section 2.4.1. Fillets were placed on a glass plate, a halogen line light (line width approx. 5 cm) was placed below the plate, and the camera was placed 1 meter above the plate. The line light was tilted approximately 15 degrees to avoid direct light reaching the camera. This transillumination setup is very similar to that described in (Agnar Holten Sivertsen et al. 2011).

An example image from the SWIR camera imaging is shown in Figure 26 a). For comparison, an interactance image of the same fillet is shown in Figure 26 b), and in Figure 26 c), the same image is shown with nematode locations indicated. The following observations can be made:

- In the SWIR transmission mode image, the amount of light is very dependent on the fillet thickness. In the thinnest areas, seen as white in the image, the camera sensor saturates, and all contrast is lost. In the thicker parts of the fillet, light transmission is very low, signal-to-noise levels are low, and the fillet appears dark. It is possible to manipulate image intensity to "flatten" the image, but the large variations in light intensity due to thickness variations is an inherent problem of this imaging mode. This problem makes it difficult to fit information from the whole fillet within the dynamic range of a single camera.
- Some of the larger nematodes are visible in the SWIR image, but there are several which are visible in the interactance image which cannot be seen clearly. Also, the main point of using SWIR transmission imaging is detecting nematodes deeply embedded in the fish muscle (not seen in interactance image, marked as magenta). However, none of these nematodes can be seen.

---

[10] http://www.hyspex.no/products/swir_384.php

- There are structures in the fish muscle causing variation in the scattering properties. It is difficult to clearly separate between such muscle structures and true nematodes.
- The horizontal resolution of the SWIR camera is approximately 0,78 mm, and the horizontal resolution of the VNIR camera (used for interactance) is 0,28 mm. This is not immediately visible in Figure 26, since the images are scaled to the same size, but it makes it difficult to detect and analyze small details.

Based on the observations listed above, Nofima decided not to pursue SWIR transmission mode imaging further, but to rather concentrate on the VIS/NIR interactance imaging, as described in the main body of the report.

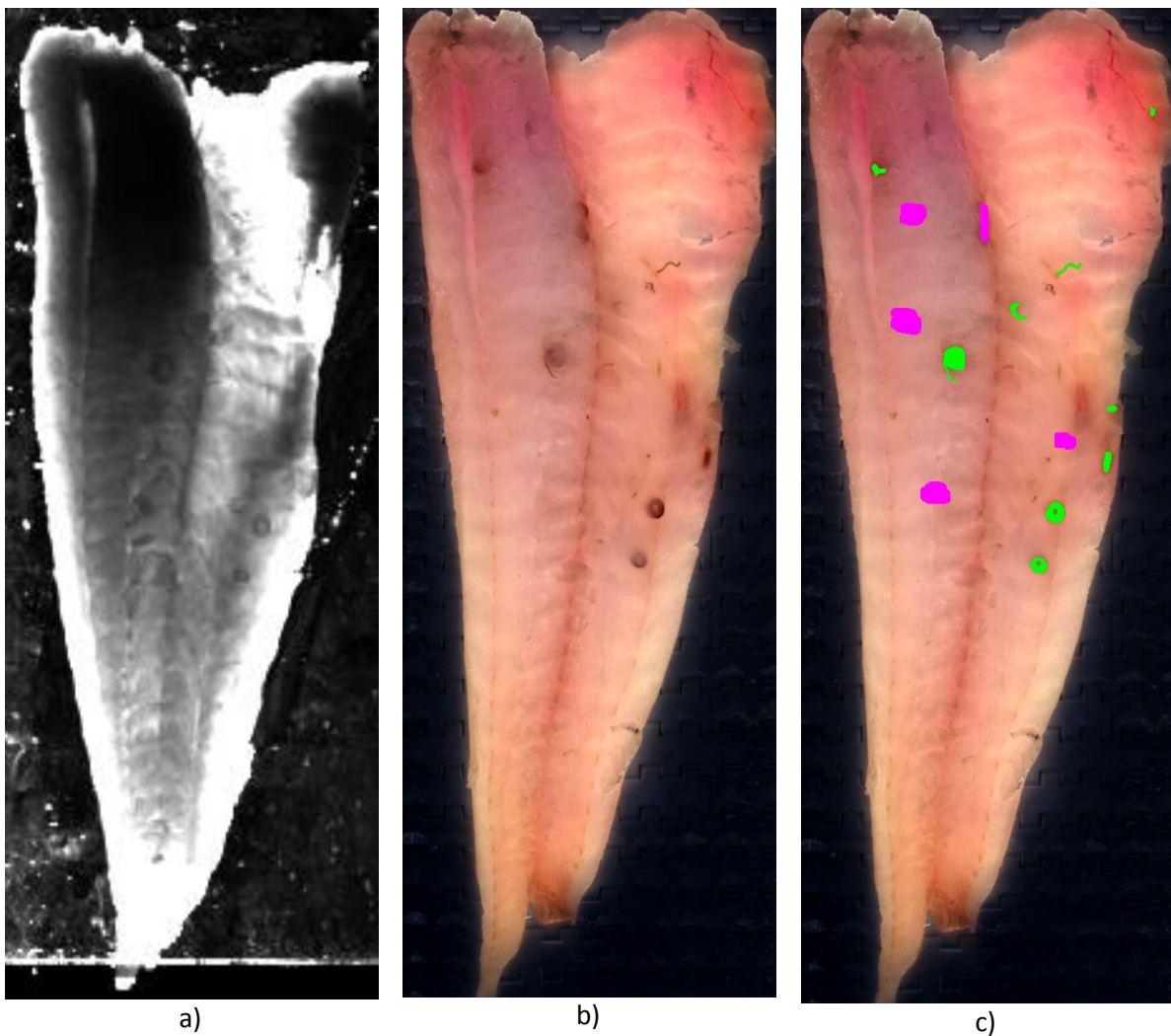a)   b)   c)

Figure 26   Example images of fillet with several nematodes. a) Image slice at 1267 nm, taken with SWIR camera. This wavelength had the highest transmission in the range close to 1300 nm. b) Synthetic color image from interactance imaging. c) Same as b), but with visible nematodes marked as green and non-visible ones marked as magenta.

9.3 Detailed Statistics for Nematode Detection for Different Preprocessing and analysis methods

In addition to the quality measures presented in the main text, the detection rate per fillet was also calculated for the table here. This was done because if there are fillets that are outliers that also have a very high number of nematodes compared to other fillets, this can potentially skew the detection results.

Details of the analysis method description are as follows. PCA indicates that the images were analysed by a PCA (all results here were PCA analysed). The next two descriptors are the type of spectral preprocessing (e.g. area normalization) and which range of wavelengths were used for analysis. HPF indicates the data was high pass filtered. If HPF appears before PCA in the name, high pass filtering was performed before PCA analysis. If HPF appears after the wavelengths, high-pass filtering was performed after PCA analysis. The final descriptor indicates which type or combination of types of classification were used.

Note that PCA was used for all variations for the following reasons:

- PCA analysis yields significant data reduction. This is needed in order to train classifiers and apply them to hyperspectral images within a reasonable amount of time (and without running out of computer memory etc.). Such data reduction will probably also be required (or at least beneficial) in an eventual industrial implementation, as it will ease the computational load for real-time data processing.
- PCA "compresses" several variables which are strongly correlated into a smaller number of uncorrelated variables. This generally improves the numerical stability and performance of the classifiers.
- PCA extracts the main variations from the spectra, while small details are discarded as noise. This makes PCA more robust to noise – at least in some cases.

Analyse Method	Min Size	Detection Rate	Detection Rate per Fillet	Detection Rate of Visible	Detection Rate of Nonvisible	Average # False Positive	Fillet without False Positive
PCA anorm 450-950 HPF LDA	10	41.4	43.6	55.9	11.3	6.5	2
PCA anorm 450-950 HPF LDA	5	44.4	46.7	60.5	11.3	11.3	1
PCA anorm 450-950 HPF SVM	10	46.3	50.4	59.6	18.8	25.6	0
PCA anorm 450-950 HPF SVM	5	53.1	55.8	67.8	22.6	41.1	0
PCA anorm 450-950 HPF SVM Cleaned	10	45.1	49.6	56.9	20.7	22.4	2
PCA anorm 450-950 HPF SVM Cleaned	5	50	52.8	61.5	26.4	35.6	0
PCA anorm 450-950 HPF LDA SVM	10	37.7	41.2	51.4	9.4	3.2	4
PCA anorm 450-950 HPF LDA SVM	5	37.7	41.2	51.4	9.4	5.7	2
PCA none 450-950 HPF LDA	10	36.4	38.5	41.9	11.3	10.6	0
PCA none 450-950 HPF LDA	5	40.1	41.2	53.2	13.2	17.1	0
PCA none 450-950 HPF SVM	10	53.1	59.2	63.3	32.1	65.9	0
PCA none 450-950 HPF SVM	5	58	62.5	70.7	32.1	105.7	0
PCA none 450-950 HPF SVM Cleaned	10	36.4	39.6	44.9	18.9	46	0
PCA none 450-950 HPF SVM Cleaned	5	46.3	49.6	56.0	26.4	73	0
PCA none 450-950 HPF LDA SVM	10	34	36	44.0	13.2	9.4	0
PCA none 450-950 HPF LDA SVM	5	34.6	36.4	45.0	13.2	15.5	0
PCA snv 450-950 HPF LDA	10	36.4	38.2	49.6	9.4	4.4	6
PCA snv 450-950 HPF LDA	5	39.5	41	53.2	11.3	7.2	5
PCA snv 450-950 HPF SVM	10	46.9	43.5	56.0	28.3	42.6	0
PCA snv 450-950 HPF SVM	5	53.1	49.8	62.4	34.0	70.6	0
PCA snv 450-950 HPF SVM Cleaned	10	40.7	36	47.7	26.4	32.5	0
PCA snv 450-950 HPF SVM Cleaned	5	46.9	46.4	54.2	32.1	52.6	0
PCA snv 450-950 HPF LDA SVM	10	30.8	29.4	43.1	5.7	3	6
PCA snv 450-950 HPF LDA SVM	5	34.6	34.5	46.8	9.4	4.9	6
HPF PCA none 450-950 LDA	10	16.7	21.3	21.1	7.6	3.9	11
HPF PCA none 450-950 LDA	5	22.8	30.4	30.3	7.6	5.2	8
HPF PCA none 450-950 SVM	10	22.8	21.5	27.5	13.2	9.2	5
HPF PCA none 450-950 SVM	5	27.8	25.1	34.8	13.2	17.1	3
HPF PCA none 450-950 SVM Cleaned	10	19.8	19.6	21.1	15.9	20.6	2
HPF PCA none 450-950 SVM Cleaned	5	27.8	26.1	30.3	22.6	33.5	1
HPF PCA none 450-950 LDA SVM	10	11.7	14.3	15.6	3.8	1.6	17
HPF PCA none 450-950 LDA SVM	5	16.7	18.8	22.9	3.8	2.6	14

9.4 Detailed Statistics for Nematode Detection for Different Preprocessing and analysis methods for Resampled Data

The comments in section 9.3 also apply to this section.

Analyse Method	Min Size	Detection Rate	Detection Rate per Fillet	Detection Rate of Visible	Detection Rate of Nonvisible	Average # False Positive	Fillet without False Positive
PCA anorm 450-950 HPF LDA	10	41.3	42.1	56.8	9.4	4.3	3
PCA anorm 450-950 HPF LDA	5	45.8	46.8	62.6	11.3	7.6	1
PCA anorm 450-950 HPF SVM	10	43.5	43.9	59.2	11.3	17.2	1
PCA anorm 450-950 HPF SVM	5	49.2	50	64.9	17.0	31.3	0
PCA none 450-950 HPF LDA	10	32.8	33.2	46.0	5.7	4.2	4
PCA none 450-950 HPF LDA	5	34.6	35.2	48.7	5.7	7.6	1
PCA none 450-950 HPF SVM	10	30.4	27.4	40.6	9.4	35.4	0
PCA none 450-950 HPF SVM	5	38.3	39.4	48.7	17.0	62.3	0
PCA snv 450-950 HPF LDA	10	22.2	18.8	31.2	3.8	2	13
PCA snv 450-950 HPF LDA	5	26.3	22.1	37.3	3.8	4	9
PCA snv 450-950 HPF SVM	10	15.5	12.9	20.3	5.6	12.5	2
PCA snv 450-950 HPF SVM	5	21.7	17.7	29.5	5.6	23.5	0